

Nonsmooth Quasistatic Modeling of Hydraulic Actuators

Ryo Kikuuwe^{*§}, Tomofumi Okada^{†‡}, Hideo Yoshihara[†],
Takayuki Doi[‡], Takao Nanjo[‡] and Koji Yamashita[‡]

February 24, 2021

Abstract

This article presents a quasistatic model of a hydraulic actuator driven by a four-valve independent metering circuit. The presented model describes the quasistatic balance between the velocity and force and that between the flowrate and the pressure. In such balanced states, the pressure difference across each valve determines the oil flowrate through the valve, the oil flowrate into the actuator determines the velocity of the actuator, and the pressures in the actuator chambers are algebraically related to the external force acting on the actuator. Based on these relations, we derive a set of quasistatic representations, which analytically relates the control valve openings, the actuator velocity, and the external force. This analytical expression is written with nonsmooth functions, of which the return values are set-valued instead of single-valued. We also show a method of incorporating the obtained nonsmooth quasistatic model into multibody simulators, in which a virtual viscoelastic element is used to mimic transient responses. In addition, the proposed model is extended to include a regeneration pipeline and to deal with a collection of actuators driven by a single pump.

Keywords: nonsmooth hydraulics, differential-algebraic relaxation, hydraulic cylinders

1 Introduction

Control technology for construction machines requires continuing research and development for future applications, such as remote and semi-automatic operation. The productivity of research and development heavily depends on simulation techniques. In particular, hydraulic actuators and hydraulic circuits are important components of construction machines, of which the physical behaviors need to be appropriately modeled in simulators. The behavior of a hydraulic actuator is highly involving, depending on the oil supply from the pump, the external forces acting on the actuator, and the states and the characteristics of many valves in the circuit.

Many of the previous studies on the modeling of hydraulic systems assume that the pressure is governed by first-order dynamics. The circuit is often divided into several oil volumes, such as those in the circuit pipelines and the actuator chambers. In each volume, the rate-of-change of the pressure is determined by the oil flowrates in and out of the volume. Such an approach, sometimes referred to as a lumped fluid approach, has been employed for the controller design

^{*}Graduate School of Advanced Science and Engineering, Hiroshima University, 1-4-1 Kagamiyama, Higashi-Hiroshima, Hiroshima 739-8527, Japan. e-mail: kikuuwe@ieee.org

[†]Kobelco Construction Machinery Dream-Driven Co-Creation Research Center, Hiroshima University, 1-4-1 Kagamiyama, Higashi-Hiroshima, Hiroshima 739-8527, Japan.

[‡]Kobelco Construction Machinery Co., Ltd., 2-2-1 Itsukaichiko, Saeki-ku, Hiroshima 731-5161, Japan.

[§]Corresponding Author

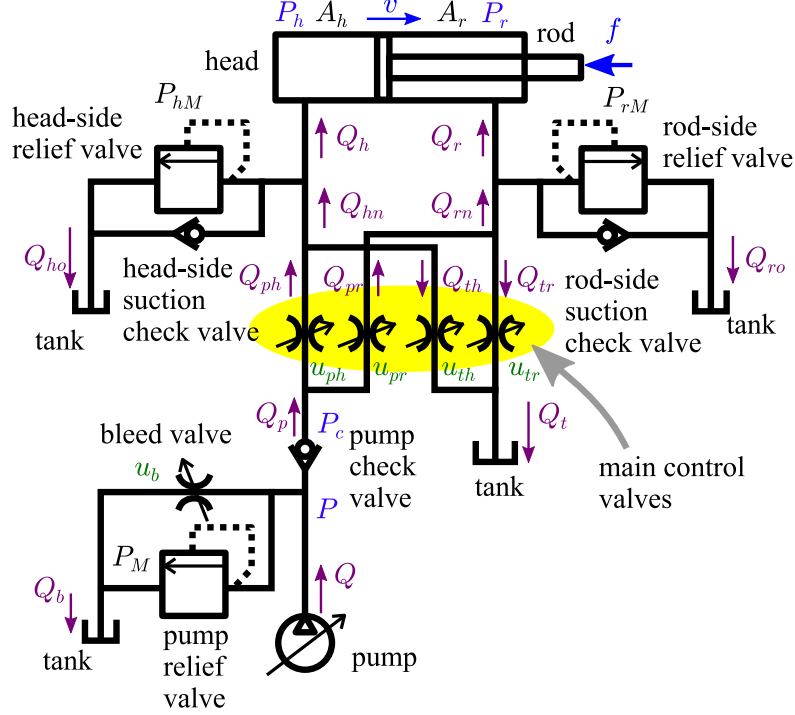


Figure 1: Hydraulic actuator and its circuit.

[7, 8, 23, 32] and for simulation purposes [24, 34]. Coupling of hydraulic systems and multibody systems have also been studied [20–22, 34].

In the conventional model of the pressure dynamics, the rate-of-change of the pressure is proportional to the bulk modulus divided by the volume of the oil. The bulk modulus of the oil is usually high, and the oil volume may be small when one needs to deal with a small segment in the pipes and when the piston approaches either end of the cylinder. Therefore, the differential equations representing the pressure dynamics can become numerically stiff, demanding a small timestep size and a high computational cost for use in simulation. Some researchers [13, 21, 28] applied the singular perturbation theory to avoid the numerical stiffness of the governing differential equations of the pressure. In the singular perturbation approach, the pressure dynamics is assumed to be so fast that the steady-state pressures are quickly achieved. Following this notion, the pressure rate-of-change in the governing differential equation is replaced by zero, and the pressure dynamics is converted into an algebraic constraint determining the steady-state pressure. Kiani Oshtorjani et al. [13] have explored the applicability of this scheme to distinguish which pressure rates-of-change can or cannot be zeroed based on the exponential stability of the original differential equation of the pressure dynamics.

This article proposes a computationally-efficient modeling scheme for hydraulic actuators, particularly focusing on the circuit structure shown in Fig. 1. This approach focuses on the quasistatic¹ balances established at the steady state, at which the pressure difference across each valve determines the oil flowrate through the valve, the oil flowrate into the actuator determines the actuator’s velocity, the pressures in the actuator chambers determine the force generated by the actuator, and the generated force equals the external force acting on the actuator. This article elaborately derives an analytical expression of the quasistatic relation between the actuator velocity and the external force from the quasistatic representations of all

¹We use the term ‘quasistatic’ because the model does not involve the pressure dynamics but involves the motion of the actuator and the oil.

valves in the circuit. One important feature of the presented expression is that it is nonsmooth, allowing for the set-valuedness of the pressure especially when the valves are closed or the actuator is stopped.

The presented approach may be viewed as a full application of the singular perturbation theory in the sense that it provides an approximate solution by neglecting the first-order pressure dynamics. In this approach, the pressures and flowrates are constrained algebraically, instead of through the dynamics. In contrast to previous works [13,21,28], the presented nonsmooth model allows for multiple steady states by involving the set-valuedness, and describes the quasistatic balance between the chamber pressures and the external force, to which the system should converge in the steady state.

In addition to the quasistatic model of Fig. 1, this article presents a method to use the model in multibody dynamics simulation. In simulations, the actuator model is connected with other mechanical components through a virtual viscoelastic element to deal with the set-valuedness of the actuator model. This approach is what Kikuuwe [15] has been referring to as a *differential-algebraic relaxation*, which has been applied to many nonsmooth problems by Kikuuwe and his colleagues [14, 16–18, 30, 31]. Some extensions toward more complicated circuit structures are also presented.

This article is organized as follows. Section 2 shows mathematical preliminaries, including definitions of relevant functions and some theorems and propositions. Section 3 constructs a nonsmooth quasistatic model of the hydraulic circuit of Fig. 1, which describes the algebraic relation among the valve openings, the rod velocity, and the external force. Section 4 presents an approach to incorporate the quasistatic model into multibody simulators. Section 5 presents an extended model including a regeneration pipeline, and Section 6 presents a model including multiple actuators driven by a single pump. Section 7 provides some concluding remarks.

2 Mathematical Preliminary

2.1 Some Nonsmooth Functions

In this article, \mathbb{R} denotes the set of all real numbers. This article extensively uses mathematical notations of the nonsmooth system theory, which involves set-valued functions. We use the following set-valued functions:

$$\mathcal{N}_{[A,B]}(x) \triangleq \begin{cases} [0, \infty) & \text{if } x = B \\ 0 & \text{if } x \in (A, B) \\ (-\infty, 0] & \text{if } x = A \\ \emptyset & \text{otherwise} \end{cases} \quad (1)$$

$$\text{gsgn}(a, x, b) \triangleq \begin{cases} b & \text{if } x > 0 \\ \text{cl}\{a, b\} & \text{if } x = 0 \\ a & \text{if } x < 0. \end{cases} \quad (2)$$

The definition (1) assumes $A < B$. Here, $\text{cl}\{a, b\}$ stands for the convex closure of the set $\{a, b\}$, being the closed set $[a, b]$ if $a \leq b$ and $[b, a]$ if $b \leq a$. The function $\mathcal{N}_{\mathcal{F}}(x)$ is referred to as the normal cone of the set \mathcal{F} at the point x . The function gsgn can be seen as a generalized version of the set-valued signum function. With the normal cone \mathcal{N} , the following relation holds true:

$$0 \leq x \perp y \geq 0 \iff x \in -\mathcal{N}_{[0,\infty)}(y) \iff y \in -\mathcal{N}_{[0,\infty)}(x). \quad (3)$$

Each of the above three expressions means that x and y are non-positive scalars at least one of which is zero. This relation is convenient to describe the flowrate-pressure relation at check

valves. In addition, with $A < B$, the following relation holds true:

$$y \in \mathcal{N}_{[A,B]}(x) \iff x \in \text{gsng}(A, y, B). \quad (4)$$

The following function represents the projection onto a closed set:

$$\text{proj}_{[A,B]}(x) \triangleq \max(A, \min(B, x)) \quad (5)$$

where $A < B$. The normal cone and the projection have the following relation:

$$a - x \in \mathcal{N}_{\mathcal{A}}(x) \iff x = \text{proj}_{\mathcal{A}}(a), \quad (6)$$

which has been shown in previous publications [5, Proposition 2] [2, Section A.3]. This article uses the following theorem:

Theorem 1. *Let $x \in \mathbb{R}$ and let $\mathcal{A} \subset \mathbb{R}$ be a closed subset of \mathbb{R} . Let $f : \mathbb{R} \rightarrow \mathbb{R}$ be a strictly decreasing function. Let $x_f \in \mathbb{R}$ satisfy $f(x_f) = 0$. Then, the following statement holds true:*

$$f(x) \in \mathcal{N}_{\mathcal{A}}(x) \iff x = \text{proj}_{\mathcal{A}}(x_f). \quad (7)$$

Proof. Because f is strictly decreasing, $x < x_f \iff f(x) < 0$, $x > x_f \iff f(x) > 0$, and $x = x_f \iff f(x) = 0$ are satisfied. This means that $f(x) \in \mathcal{N}_{\mathcal{A}}(x) \iff x_f - x \in \mathcal{N}_{\mathcal{A}}(x)$ and (6) implies that it is equivalent to $x = \text{proj}_{\mathcal{A}}(x_f)$. \square

2.2 Some Smooth Functions

The following single-valued functions are used in the article:

$$\mathcal{S}(x) \triangleq \text{sgn}(x)x^2 \quad (8)$$

$$\mathcal{R}(x) \triangleq \text{sgn}(x)\sqrt{|x|} \quad (9)$$

$$\psi(u_1, u_2) \triangleq \begin{cases} 0 & \text{if } u_1 = u_2 = 0 \\ \frac{u_1^2 u_2^2}{u_1^2 + u_2^2} & \text{otherwise.} \end{cases} \quad (10)$$

The functions \mathcal{R} and \mathcal{S} are strictly increasing continuous functions satisfying $\mathcal{R}(\mathcal{S}(x)) = \mathcal{S}(\mathcal{R}(x)) = x$. The function ψ is differentiable everywhere.

Section 4 will use the following functions:

$$\begin{aligned} \Phi_A(b, c, a) &\triangleq -\text{sgn}(c) \frac{\sqrt{a^2 b^2 + 4a|c|} - ab}{2} \quad (11) \\ \Phi_B(b, c, a_0, a_1, x_1) &\triangleq \begin{cases} -\frac{\sqrt{a_0^2(a_1 b + 2x_1)^2 + 4a_0(a_0 + a_1)(a_1 c - x_1^2)} - a_0(a_1 b + 2x_1)}{2(a_0 + a_1)} \\ \quad \text{if } (-a_0(bx + c) \leq \mathcal{S}(x_1) \leq 0) \vee (0 \leq \mathcal{S}(x_1) \leq a_1 c) \\ \frac{\sqrt{a_0^2(a_1 b - 2x_1)^2 - 4a_0(a_0 + a_1)(a_1 c + x_1^2)} - a_0(a_1 b - 2x_1)}{2(a_0 + a_1)} \\ \quad \text{if } (0 \leq \mathcal{S}(x_1) \leq -a_0(bx + c)) \vee (a_1 c \leq \mathcal{S}(x_1) \leq 0) \\ -\frac{2\sqrt{a_0}(a_1 c + x_1^2)}{\sqrt{a_0}(a_1 b - 2x_1) + \sqrt{a_0}(a_1 b - 2x_1)^2 + 4(a_1 - a_0)(a_1 c + x_1^2)} \\ \quad \text{if } \mathcal{S}(x_1) \leq \min(0, -a_0(bx + c), a_1 c) \\ \frac{2\sqrt{a_0}(x_1^2 - a_1 c)}{\sqrt{a_0}(a_1 b + 2x_1) + \sqrt{a_0}(a_1 b + 2x_1)^2 + 4(a_1 - a_0)(x_1^2 - a_1 c)} \\ \quad \text{if } \max(0, -a_0(bx_1 + c), a_1 c) \leq \mathcal{S}(x_1). \end{cases} \quad (12) \end{aligned}$$

With these functions, we have the following propositions:

Proposition 1. *Let $a \geq 0$ and $b > 0$. Then, the following statement holds true:*

$$x = \Phi_A(b, c, a) \iff \lim_{\tilde{a} \rightarrow a} \frac{\mathcal{S}(x)}{\tilde{a}} + bx + c = 0. \quad (13)$$

Proposition 2. *Let $a_0 \geq 0$, $a_1 \geq 0$, and $b > 0$, and let $a_0^2 + a_1^2 > 0$ be satisfied. Then, the following statement holds true:*

$$x = \Phi_B(b, c, a_0, a_1, x_1) \iff \lim_{\tilde{a}_0 \rightarrow a_0} \frac{\mathcal{S}(x)}{\tilde{a}_0} + \lim_{\tilde{a}_1 \rightarrow a_1} \frac{\mathcal{S}(x - x_1)}{\tilde{a}_1} + bx + c = 0. \quad (14)$$

The proofs of these propositions can be obtained through tedious but straightforward derivations.

We also use the following theorems, of which the proofs are rather trivial:

Theorem 2. *Let $f : \mathbb{R} \rightarrow \mathbb{R}$ and $g : \mathbb{R} \rightarrow \mathbb{R}$ be strictly decreasing functions and let $g(0) \leq f(0)$ be satisfied. Let x_f and x_g satisfy $b = f(x_f)$ and $b = g(x_g)$ where $b \in \mathbb{R}$. Then, the following statement holds true:*

$$b \in \text{gsgn}(f(x), x, g(x)) \iff x = \begin{cases} x_f & \text{if } b > f(0) \\ x_g & \text{if } b < g(0) \\ 0 & \text{otherwise.} \end{cases} \quad (15)$$

Theorem 3. *Let $f_1 : \mathbb{R} \rightarrow \mathbb{R}$ and $f_2 : \mathbb{R} \rightarrow \mathbb{R}$ be strictly decreasing functions. Let x_i satisfy $f_i(x) = 0$ for $i \in \{1, 2\}$. Then, the following two statements hold true:*

$$\min(f_1(x), f_2(x)) = 0 \iff x = \min(x_1, x_2) \quad (16)$$

$$\max(f_1(x), f_2(x)) = 0 \iff x = \max(x_1, x_2). \quad (17)$$

3 Nonsmooth Quasistatic Model

This section considers the hydraulic circuit illustrated in Fig. 1, which is a four-valve independent metering circuit to drive a double-acting hydraulic actuator. The actuator has two chambers separated by the piston, and the motion of the piston is extracted as the motion of the rod, which applies forces to external objects. We are interested in the quasistatic relation among the rod velocity v , positive when the rod is extending, the external force f , positive when it is compressing the rod, and the opening ratios of the valves. This hydraulic circuit is similar to those studied in, e.g., [6, 9, 25–27], where the quasistatic relations are also considered. Our main contribution lies in an elaborate analytical representation of the whole circuit, which is rather complicated than those in previous studies, using the nonsmooth formalism to deal with relief valves and check valves.

This article uses the terminology for linear hydraulic actuators (i.e., hydraulic cylinders), but the presented approach is applicable also to rotary hydraulic actuators by replacing the velocity and the external force by the angular velocity and the torque, respectively.

3.1 Quasistatic Relations

In Fig. 1, Q_* and P_* denote the flowrates and the pressure at each point. The pump provides the flowrate Q to the circuit via a pump check valve and two of the four main control valves. These control valves are connected to the head-side and the rod-side chambers of the actuator. The chambers are also connected to the tank with the zero pressure via the other two control

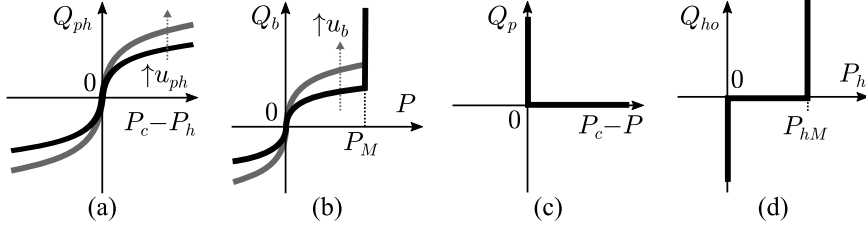


Figure 2: Flowrate-pressure relations at: (a) one of main control valves (19h), (b) the bleed and the pump relief valves (19l), (c) the pump check valve (19m), and (d) the head-side relief and the suction check valves (19n).

valves. Each chamber of the actuator also connects to the tank through a parallel combination of a relief valve and a check valve, which are named as indicated in the figure. There is another control valve, referred to as a bleed valve, and it leads to the tank in parallel to a relief valve, referred to as a pump relief valve.

The degrees of the opening of the valves are represented by dimensionless variables $u_* \in [0, 1]$ ($* \in \{ph, tr, pr, th, b\}$), which are the ratios of the valve opening areas to their maximum values. The control valves are manipulated by a controller that accepts external commands, which are given through, e.g., operation levers of an excavator. When the external command is to stop the actuator, all the four main valves are closed. When the external command is to move the actuator in the positive direction (i.e., extend the rod), both or either of u_{ph} and u_{tr} are set positive and u_{th} and u_{pr} are set zero. When the operator's command is to move the actuator in the negative direction (i.e, retract the rod), u_{ph} and u_{tr} are set zero and both or either of u_{th} and u_{pr} are set positive. Based on this idea, we assume that the vector $\mathbf{u} \triangleq [u_{ph}, u_{tr}, u_{pr}, u_{th}, u_b]^T$ always belongs to either of the following three subsets:

$$\mathbf{u}_0 \triangleq \{\mathbf{u} \in \mathbb{R}^5 \mid u_1 = u_2 = u_3 = u_4 = 0 \wedge u_5 > 0\} \quad (18a)$$

$$\mathbf{u}_+ \triangleq \{\mathbf{u} \in \mathbb{R}^5 \mid u_1^2 + u_2^2 > 0 \wedge u_3 = u_4 = 0 \wedge u_5 \geq 0\} \quad (18b)$$

$$\mathbf{u}_- \triangleq \{\mathbf{u} \in \mathbb{R}^5 \mid u_1 = u_2 = 0 \wedge u_3^2 + u_4^2 > 0 \wedge u_5 \geq 0\} \quad (18c)$$

where u_i ($i \in \{1, \dots, 5\}$) stands for the i th element of the vector \mathbf{u} .

Now, let us make an exhaustive list of algebraic relations among the pressures, the flowrates, the external force, and the actuator velocity at the steady state. First, according to the principle of mass conservation, one can see that the following relations hold true at junctions in the circuit:

$$Q_{hn} = Q_{ph} - Q_{th} \quad (19a)$$

$$Q_{rn} = Q_{pr} - Q_{tr} \quad (19b)$$

$$Q_h = Q_{hn} - Q_{ho} \quad (19c)$$

$$Q_r = Q_{rn} - Q_{ro} \quad (19d)$$

$$Q_t = Q_{th} + Q_{tr} \quad (19e)$$

$$Q_p = Q_{ph} + Q_{pr} \quad (19f)$$

$$Q_b = Q - Q_p. \quad (19g)$$

Second, let us focus on the control valves. As indicated in Fig. 1, P_h and P_r are the internal pressures of the head- and rod-side chambers, respectively, P_c is the pressure at the check valve connected to the pump, and P is the pressure at the outlet of the pump. According to the

conventional orifice model [4,7], we can assume that the following flowrate-pressure relations are satisfied:

$$Q_{ph} = c_{ph}u_{ph}\mathcal{R}(P_c - P_h) \quad (19h)$$

$$Q_{th} = c_{th}u_{th}\mathcal{R}(P_h) \quad (19i)$$

$$Q_{pr} = c_{pr}u_{pr}\mathcal{R}(P_c - P_r) \quad (19j)$$

$$Q_{tr} = c_{tr}u_{tr}\mathcal{R}(P_r) \quad (19k)$$

$$Q_b \in c_b u_b \mathcal{R}(P) + \mathcal{N}_{(-\infty, P_M]}(P). \quad (19l)$$

Fig. 2(a) illustrates the relation (19h). The coefficients c_* are defined as $c_* = C_* a_* \sqrt{2/\rho}$ ($* \in \{ph, tr, pr, th, b\}$) where C_* is the dimensionless coefficient named a discharge coefficient [19], which is typically around 0.6 or 0.7 [29, 33], a_* is the maximum opening area (m^2) of the valve, and ρ is the mass density (kg/m^3) of the oil. Equation (19l) represents the combined effect of the relief valve and the bleed valve, which limits the pump pressure up to P_M as illustrated in Fig. 2(b).

Third, let us consider the check valves and the relief valves. The check valve connected to the pump imposes the following constraint:

$$Q_p \in -\mathcal{N}_{[0, \infty)}(P_c - P), \quad (19m)$$

which means that the flowrate Q_p is zero when $P_c - P > 0$, as illustrated in Fig. 2(c). The effects of the relief valves and the suction check valves connected to the chambers are written as follows:

$$Q_{ho} \in \mathcal{N}_{[0, P_{hM}]}(P_h) \quad (19n)$$

$$Q_{ro} \in \mathcal{N}_{[0, P_{rM}]}(P_r). \quad (19o)$$

Here, P_{hM} and P_{rM} are the pressure limits of the relief valves connected to the head- and rod-side chambers, respectively. These expressions mean that P_h and P_r are always in the ranges of $[0, P_{hM}]$ and $[0, P_{rM}]$, respectively, as illustrated in Fig. 2(d). When the pressure reaches the upper limit, the oil flows into the tank. When the pressure reaches zero, the oil is drawn into the chamber from the tank.

Lastly, we discuss the actuator. Let A_h and A_r be the cross-sectional areas of the head- and rod-side chambers, respectively. Then, at the steady state where the rod inertia can be neglected, the constraints imposed by the actuator can be written as follows:

$$v = Q_h/A_h \quad (19p)$$

$$v = -Q_r/A_r \quad (19q)$$

$$f = A_h P_h - A_r P_r. \quad (19r)$$

If one deals with rotary actuators, both A_r and A_h (measured in m^2) should be replaced by the volume displacement per one radian of rotation, which is measured in m^3/rad .

In conclusion, now we have 18 algebraic constraints in (19) and 19 variables, which are listed as follows

- $\{Q_{ho}, Q_{ro}, Q_{hn}, Q_{rn}, Q_h, Q_r, Q_{ph}, Q_{pr}, Q_{th}, Q_{tr}, Q_t, Q_p, Q_b\}$: 13 flowrate values
- $\{P, P_h, P_r, P_c\}$: 4 pressure values
- $\{f, v\}$: the external force to the rod and the velocity of the rod.

Remark 1. *The presented formalism can be said to be close to the classical hydraulic-electric analogy [10, 12], which replaces the pressure and the flowrate by the voltage and the current, respectively. Considering that the presented approach involves the nonsmoothness, it is also analogous to the nonsmooth electronics [1, 3, 11]. In this analogy, a check valve, for example, corresponds to an ideal diode [1].*

3.2 Normalized Representations

For the convenience of derivation, we now normalize some quantities in the following manner:

$$q_* \triangleq Q_*/A_h \quad (* \in \{ho, hn, h, ph, th\}), \quad \hat{u}_* \triangleq c_* u_*/A_h^{3/2} \quad (* \in \{ph, th\}) \quad (20)$$

$$q_* \triangleq Q_*/A_r \quad (* \in \{ro, rn, r, pr, tr\}), \quad \hat{u}_* \triangleq c_* u_*/A_r^{3/2} \quad (* \in \{pr, tr\}) \quad (21)$$

$$F_* \triangleq P_* A_*, \quad F_{*M} = P_{*M} A_* \quad (* \in \{h, r\}) \quad (22)$$

$$U_b \triangleq c_b u_b. \quad (23)$$

The regularized input vector is defined as $\hat{\mathbf{u}} = [\hat{u}_{ph}, \hat{u}_{tr}, \hat{u}_{pr}, \hat{u}_{th}, U_b]^T$. By using these definitions, (19) can be rewritten as follows:

$$q_{hn} = q_{ph} - q_{th} \quad (24a)$$

$$q_{rn} = q_{pr} - q_{tr} \quad (24b)$$

$$q_h = q_{hn} - q_{ho} \quad (24c)$$

$$q_r = q_{rn} - q_{ro} \quad (24d)$$

$$Q_t = A_h q_{th} + A_r q_{tr} \quad (24e)$$

$$Q_p = A_h q_{ph} + A_r q_{pr} \quad (24f)$$

$$Q_b = Q - Q_p \quad (24g)$$

$$q_{ph} = \hat{u}_{ph} \mathcal{R}(A_h P_c - F_h) \quad (24h)$$

$$q_{th} = \hat{u}_{th} \mathcal{R}(F_h) \quad (24i)$$

$$q_{pr} = \hat{u}_{pr} \mathcal{R}(A_r P_c - F_r) \quad (24j)$$

$$q_{tr} = \hat{u}_{tr} \mathcal{R}(F_r) \quad (24k)$$

$$Q_b \in U_b \mathcal{R}(P) + \mathcal{N}_{(-\infty, P_M]}(P) \quad (24l)$$

$$Q_p \in \mathcal{N}_{(-\infty, P_c]}(P) \quad (24m)$$

$$q_{ho} \in \mathcal{N}_{[0, F_{hM}]}(F_h) \quad (24n)$$

$$q_{ro} \in \mathcal{N}_{[0, F_{rM}]}(F_r) \quad (24o)$$

$$v = q_h \quad (24p)$$

$$v = -q_r \quad (24q)$$

$$f = F_h - F_r. \quad (24r)$$

Note that the equivalence between (19m) and (24m) can be derived from the definition of the normal cone.

Now, let us attempt to reduce the number of variables. Substituting (24m) and (24g) into (24l) yields

$$\begin{aligned} Q &\in \mathcal{N}_{(-\infty, P_c]}(P) + U_b \mathcal{R}(P) + \mathcal{N}_{(-\infty, P_M]}(P) \\ &= U_b \mathcal{R}(P) + \mathcal{N}_{(-\infty, \min(P_c, P_M)]}(P), \end{aligned} \quad (25)$$

which is equivalent to

$$P = \min(P_c, P_M, \mathcal{S}(Q/U_b)) \quad (26)$$

because of Theorem 1. Since $q_h = -q_r = v$, we can eliminate the two variables q_h and q_r . Moreover, q_{ho} , q_{ro} , q_{hn} , q_{rn} , q_{ph} , q_{th} , q_{pr} , q_{tr} , and Q_t can also be eliminated. This gives the following five equations for the four variables $\{P, P_c, F_h, F_r, f\}$:

$$-v + \hat{u}_{ph}\mathcal{R}(A_h P_c - F_h) - \hat{u}_{th}\mathcal{R}(F_h) \in \mathcal{N}_{[0, F_{hM}]}(F_h) \quad (27a)$$

$$v + \hat{u}_{pr}\mathcal{R}(A_r P_c - F_r) - \hat{u}_{tr}\mathcal{R}(F_r) \in \mathcal{N}_{[0, F_{rM}]}(F_r) \quad (27b)$$

$$A_h \hat{u}_{ph}\mathcal{R}(A_h P_c - F_h) + A_r \hat{u}_{pr}\mathcal{R}(A_r P_c - F_r) \in \mathcal{N}_{(-\infty, P_c]}(P) \quad (27c)$$

$$Q \in U_b \mathcal{R}(P) + A_h \hat{u}_{ph}\mathcal{R}(A_h P_c - F_h) + A_r \hat{u}_{pr}\mathcal{R}(A_r P_c - F_r) + \mathcal{N}_{(-\infty, P_M]}(P) \quad (27d)$$

$$f = F_h - F_r. \quad (27e)$$

3.3 Main Result: Nonsmooth Quasistatic Map from v to f

Now we derive the relation between f and v from (27). If $\hat{u} \in \mathbf{U}_0$, (27) reduces to the following:

$$-v \in \mathcal{N}_{[0, F_{hM}]}(F_h) \quad (28a)$$

$$v \in \mathcal{N}_{[0, F_{rM}]}(F_r) \quad (28b)$$

$$0 \in \mathcal{N}_{(-\infty, P_c]}(P) \quad (28c)$$

$$Q \in U_b \mathcal{R}(P) + \mathcal{N}_{(-\infty, P_M]}(P) \quad (28d)$$

$$f = F_h - F_r, \quad (28e)$$

from which

$$F_h \in \text{gsgn}(F_{hM}, v, 0), \quad F_r \in \text{gsgn}(0, v, F_{rM}) \quad (29)$$

and $f \in \text{gsgn}(F_{hM}, v, -F_{rM})$ can be derived by using (4). This means that f can take any values between F_{hM} and $-F_{rM}$ when $v = 0$, which is consistent with the fact that, when all the main control valves are closed, the cylinder holds its position by producing the reaction force against the external force as long as the relief valves are closed.

If $\hat{u} \in \mathbf{U}_+$, (27) reduces to the following:

$$-v + \hat{u}_{ph}\mathcal{R}(A_h P_c - F_h) \in \mathcal{N}_{[0, F_{hM}]}(F_h) \quad (30a)$$

$$v - \hat{u}_{tr}\mathcal{R}(F_r) \in \mathcal{N}_{[0, F_{rM}]}(F_r) \quad (30b)$$

$$A_h \hat{u}_{ph}\mathcal{R}(A_h P_c - F_h) \in \mathcal{N}_{(-\infty, P_c]}(P) \quad (30c)$$

$$Q \in U_b \mathcal{R}(P) + A_h \hat{u}_{ph}\mathcal{R}(A_h P_c - F_h) + \mathcal{N}_{(-\infty, P_M]}(P) \quad (30d)$$

$$f = F_h - F_r. \quad (30e)$$

Here, (30a), (30b) and (30c) can be rewritten as

$$F_h = \text{proj}_{[0, F_{hM}]}(A_h P_c - \mathcal{S}(v)/\hat{u}_{ph}^2) \quad (31)$$

$$F_r = \text{proj}_{[0, F_{rM}]}(\mathcal{S}(v)/\hat{u}_{tr}^2) \quad (32)$$

$$P_c = \max(P, F_h/A_h), \quad (33)$$

respectively, because of Theorem 1. Substituting (33) into (31) and (30d) results in:

$$F_h = \text{proj}_{[0, F_{hM}]}(\max(A_h P, F_h) - \mathcal{S}(v)/\hat{u}_{ph}^2). \quad (34a)$$

$$Q \in U_b \mathcal{R}(P) + A_h \hat{u}_{ph}\mathcal{R}(\max(A_h P - F_h, 0)) + \mathcal{N}_{(-\infty, P_M]}(P), \quad (34b)$$

respectively. Now F_r is obtained by (32), and thus we focus on obtaining F_h from (34). If $v < 0$, (34a) implies $F_h = F_{hM}$. If $v = 0$, (34a) implies that $\min(A_h P, F_{hM}) \leq F_h \leq F_{hM}$. If $v = 0$ and

$F_h < F_{hM}$, (34a) implies $F_h \geq A_h P$ and substituting it into (34b) yields $P = \min(P_M, Q^2/U_b^2)$. Therefore, if $v = 0$, the condition (34) implies the following:

$$F_h \in [\min(F_{hM}, A_h P_M, A_h Q^2/U_b^2), F_{hM}]. \quad (35)$$

If $v > 0$, (34a) implies $A_h P > F_h$ and thus (34) can be rewritten as follows:

$$F_h = \text{proj}_{[0, F_{hM}]}(A_h P - \mathcal{S}(v)/\hat{u}_{ph}^2). \quad (36a)$$

$$Q \in U_b \mathcal{R}(P) + A_h \hat{u}_{ph} \mathcal{R}(A_h P - \text{proj}_{[0, F_{hM}]}(A_h P - \mathcal{S}(v)/\hat{u}_{ph}^2)) + \mathcal{N}_{(-\infty, P_M]}(P). \quad (36b)$$

The relation (36b) implies that P is a strictly increasing function of Q that saturates at $P = P_M$. As long as $A_h P - \mathcal{S}(v)/\hat{u}_{ph}^2 \in [0, F_{hM}]$, P is written as

$$P = \min\left(P_M, -\frac{A_h^2}{U_b^2} \mathcal{S}\left(v - \frac{Q}{A_h}\right)\right). \quad (37)$$

Outside this range, P is expressed as another function of Q that strictly increases with respect to Q and continuously connects to (37). The value of P outside the range does not influence F_h because F_h is saturated at 0 and F_{hM} due to (36a). Therefore, if $v > 0$, the condition (34) implies

$$F_h = \text{proj}_{[0, F_{hM}]} \left(\min\left(A_h P_M, -\frac{A_h^3}{U_b^2} \mathcal{S}\left(v - \frac{Q}{A_h}\right)\right) - \frac{\mathcal{S}(v)}{\hat{u}_{ph}^2} \right), \quad (38)$$

which is obtained by substituting (37) into (36a). Unifying the three cases, i.e., $F_h = F_{hM}$ for $v < 0$, (35) for $v = 0$, and (38) for $v > 0$, we have the following expression for the case $\hat{\mathbf{u}} \in \mathbf{U}_+$:

$$F_h \in \text{gsgn} \left(F_{hM}, v, \text{proj}_{[0, F_{hM}]} \left(\min\left(A_h P_M, -\frac{A_h^3}{U_b^2} \mathcal{S}\left(v - \frac{Q}{A_h}\right)\right) - \frac{\mathcal{S}(v)}{\hat{u}_{ph}^2} \right) \right). \quad (39)$$

If $\hat{\mathbf{u}} \in \mathbf{U}_-$, we have

$$F_h = \text{proj}_{[0, F_{hM}]}(-\mathcal{S}(v)/\hat{u}_{th}^2) \quad (40)$$

for any v in the same manner as (32). Combining (40) for $\hat{\mathbf{u}} \in \mathbf{U}_-$, (39) for $\hat{\mathbf{u}} \in \mathbf{U}_+$ and (29) for $\hat{\mathbf{u}} \in \mathbf{U}_0$, we have

$$F_h \in \Gamma_h(v) \triangleq \text{gsgn}(\Gamma_{h-}(v), v, \Gamma_{h+}(v)) \quad (41a)$$

where

$$\Gamma_{h+}(v) \triangleq \text{proj}_{[0, F_{hM}]} \left(\min\left(A_h P_M, -\frac{A_h^3}{U_b^2} \mathcal{S}\left(v - \frac{Q}{A_h}\right)\right) - \frac{\mathcal{S}(v)}{\hat{u}_{ph}^2} \right) \quad (41b)$$

$$\Gamma_{h-}(v) \triangleq \text{proj}_{[0, F_{hM}]} \left(-\frac{\mathcal{S}(v)}{\hat{u}_{th}^2} \right) \quad (41c)$$

for any $\hat{\mathbf{u}}$. In the same manner, F_r for any $\hat{\mathbf{u}}$ is obtained as follows:

$$F_r \in \Gamma_r(v) \triangleq \text{gsgn}(\Gamma_{r-}(v), v, \Gamma_{r+}(v)) \quad (42a)$$

where

$$\Gamma_{r+}(v) \triangleq \text{proj}_{[0, F_{rM}]} \left(\frac{\mathcal{S}(v)}{\hat{u}_{tr}^2} \right) \quad (42b)$$

$$\Gamma_{r-}(v) \triangleq \text{proj}_{[0, F_{rM}]} \left(\min\left(A_r P_M, \frac{A_r^3}{U_b^2} \mathcal{S}\left(v + \frac{Q}{A_r}\right)\right) + \frac{\mathcal{S}(v)}{\hat{u}_{pr}^2} \right). \quad (42c)$$

By using (41) and (42), the relation between v and f is obtained as follows:

$$f \in \Gamma(v) \triangleq \Gamma_h(v) - \Gamma_r(v). \quad (43)$$

For the convenience of further derivations, we can also write the set-valued map $\Gamma(v)$ in the following form:

$$\Gamma(v) = \text{gsgn}(\Gamma_-(v), v, \Gamma_+(v)) \quad (44a)$$

where

$$\Gamma_+(v) \triangleq \Gamma_{h+}(v) - \Gamma_{r+}(v) \quad (44b)$$

$$= \max(\min(\max(\Gamma_{+0a}(v), \Gamma_{+0b}(v)), \max(\Gamma_{+1a}(v), \Gamma_{+1b}(v)), \max(\Gamma_{+2a}(v), \Gamma_{+2b}(v))), \Gamma_{+3}(v), -F_{rM}) \quad (44c)$$

$$\Gamma_-(v) \triangleq \Gamma_{h-}(v) - \Gamma_{r-}(v) \quad (44d)$$

$$= \min(\max(\min(\Gamma_{-0a}(v), \Gamma_{-0b}(v)), \min(\Gamma_{-1a}(v), \Gamma_{-1b}(v)), \min(\Gamma_{-2a}(v), \Gamma_{-2b}(v))), \Gamma_{-3}(v), F_{hM}) \quad (44e)$$

$$\Gamma_{+0a}(v) \triangleq F_{hM} - \frac{\mathcal{S}(v)}{\hat{u}_{tr}^2} \quad (44f)$$

$$\Gamma_{+0b}(v) \triangleq F_{hM} - F_{rM} \quad (44g)$$

$$\Gamma_{+1a}(v) \triangleq -\frac{A_h^3}{U_b^2} \mathcal{S}\left(v - \frac{Q}{A_h}\right) - \frac{\mathcal{S}(v)}{\hat{u}_{ph}^2} - \frac{\mathcal{S}(v)}{\hat{u}_{tr}^2} \quad (44h)$$

$$\Gamma_{+1b}(v) \triangleq -\frac{A_h^3}{U_b^2} \mathcal{S}\left(v - \frac{Q}{A_h}\right) - \frac{\mathcal{S}(v)}{\hat{u}_{ph}^2} - F_{rM} \quad (44i)$$

$$\Gamma_{+2a}(v) \triangleq A_h P_M - \frac{\mathcal{S}(v)}{\hat{u}_{ph}^2} - \frac{\mathcal{S}(v)}{\hat{u}_{tr}^2} \quad (44j)$$

$$\Gamma_{+2b}(v) \triangleq A_h P_M - \frac{\mathcal{S}(v)}{\hat{u}_{ph}^2} - F_{rM} \quad (44k)$$

$$\Gamma_{+3}(v) \triangleq -\frac{\mathcal{S}(v)}{\hat{u}_{tr}^2} \quad (44l)$$

$$\Gamma_{-0a}(v) \triangleq -F_{rM} - \frac{\mathcal{S}(v)}{\hat{u}_{th}^2} \quad (44m)$$

$$\Gamma_{-0b}(v) \triangleq -F_{rM} + F_{hM} \quad (44n)$$

$$\Gamma_{-1a}(v) \triangleq -\frac{A_r^3}{U_b^2} \mathcal{S}\left(v + \frac{Q}{A_r}\right) - \frac{\mathcal{S}(v)}{\hat{u}_{pr}^2} - \frac{\mathcal{S}(v)}{\hat{u}_{th}^2} \quad (44o)$$

$$\Gamma_{-1b}(v) \triangleq -\frac{A_r^3}{U_b^2} \mathcal{S}\left(v + \frac{Q}{A_r}\right) - \frac{\mathcal{S}(v)}{\hat{u}_{pr}^2} + F_{hM} \quad (44p)$$

$$\Gamma_{-2a}(v) \triangleq -A_r P_M - \frac{\mathcal{S}(v)}{\hat{u}_{pr}^2} - \frac{\mathcal{S}(v)}{\hat{u}_{th}^2} \quad (44q)$$

$$\Gamma_{-2b}(v) \triangleq -A_r P_M - \frac{\mathcal{S}(v)}{\hat{u}_{pr}^2} + F_{hM} \quad (44r)$$

$$\Gamma_{-3}(v) \triangleq -\frac{\mathcal{S}(v)}{\hat{u}_{th}^2}. \quad (44s)$$

Here, the divisions by \hat{u}_*^2 or U_b^2 do not cause troubles even when they are zeros because (44c) implicitly includes upper and lower bounds. One workaround in the implementation may be to

Table 1: States of valves at each segment of $\Gamma(v)$. hR = head-side relief valve; hSC = head-side suction check valve; pR = pump relief valve; rSC = rod-side suction relief valve; rR = rod-side relief valve; o = open; x = closed; - = either open or closed.

Γ	v	\hat{u}	hR	hSC	pR	rSC	rR
$-F_{rM}$	+	$\mathcal{U}_+ \cup \mathcal{U}_0 \cup \mathcal{U}_-$	x	o	-	x	o
Γ_{+3}	+	\mathcal{U}_+	x	o	-	x	x
Γ_{+2b}	+	\mathcal{U}_+	x	x	o	x	o
Γ_{+2a}	+	\mathcal{U}_+	x	x	o	x	x
Γ_{+1b}	+	\mathcal{U}_+	x	x	x	x	o
Γ_{+1a}	+	\mathcal{U}_+	x	x	x	x	x
Γ_{+0b}	+	\mathcal{U}_+	o	x	-	x	o
Γ_{+0a}	+	\mathcal{U}_+	o	x	-	x	x
$[\Gamma_+(0), F_{hM}]$	0	\mathcal{U}_+	x	x	-	x	x
$[-F_{rM}, F_{hM}]$	0	\mathcal{U}_0	x	x	-	x	x
$[-F_{rM}, \Gamma_-(0)]$	0	\mathcal{U}_-	x	x	-	x	x
Γ_{-0a}	-	\mathcal{U}_-	x	x	-	x	o
Γ_{-0b}	-	\mathcal{U}_-	o	x	-	x	o
Γ_{-1a}	-	\mathcal{U}_-	x	x	x	x	x
Γ_{-1b}	-	\mathcal{U}_-	o	x	x	x	x
Γ_{-2a}	-	\mathcal{U}_-	x	x	o	x	x
Γ_{-2b}	-	\mathcal{U}_-	o	x	o	x	x
Γ_{-3}	-	\mathcal{U}_-	x	x	-	o	x
F_{hM}	-	$\mathcal{U}_+ \cup \mathcal{U}_0 \cup \mathcal{U}_-$	o	x	-	o	x

replace the divisions by \hat{u}_*^2 by those by $\max(\varepsilon, \hat{u}_*^2)$ where ε is a small positive number close to the machine epsilon.

It should be noted that, at $v = 0$, the function $\Gamma(v)$ is set-valued and its value is the closed set $[\Gamma_+(0), \Gamma_-(0)]$. The boundaries $\Gamma_+(0)$ and $\Gamma_-(0)$ are obtained from a straightforward derivation as

$$\Gamma_+(0) = \Gamma_{h+}(0) - \Gamma_{r+}(0), \quad \Gamma_-(0) = \Gamma_{h-}(0) - \Gamma_{r-}(0) \quad (45a)$$

where

$$\Gamma_{h+}(0) = \begin{cases} \min(F_{hM}, A_h P_M, A_h Q^2 / U_b^2) & \text{if } \hat{u}_{ph} > 0 \\ 0 & \text{if } \hat{u}_{ph} = 0 \end{cases} \quad (45b)$$

$$\Gamma_{r+}(0) = \begin{cases} 0 & \text{if } \hat{u}_{tr} > 0 \\ F_{rM} & \text{if } \hat{u}_{tr} = 0 \end{cases} \quad (45c)$$

$$\Gamma_{h-}(0) = \begin{cases} 0 & \text{if } \hat{u}_{th} > 0 \\ F_{hM} & \text{if } \hat{u}_{th} = 0 \end{cases} \quad (45d)$$

$$\Gamma_{r-}(0) = \begin{cases} \min(F_{rM}, A_r P_M, A_r Q^2 / U_b^2) & \text{if } \hat{u}_{pr} > 0 \\ 0 & \text{if } \hat{u}_{pr} = 0. \end{cases} \quad (45e)$$

As can be seen from the expression (44), the function $\Gamma(v)$ is composed of many segments. Interestingly, each segment has a clear physical interpretation. For example, in the segments listed in (44f)-(44l), the last term, either $-F_{rM}$ or $-\mathcal{S}(v)/\hat{u}_{tr}^2$, represents the state of the rod-side relief valve, either closed or open, respectively. In this way of consideration, we can summarize the valve states at each curve segment as in Table 1.

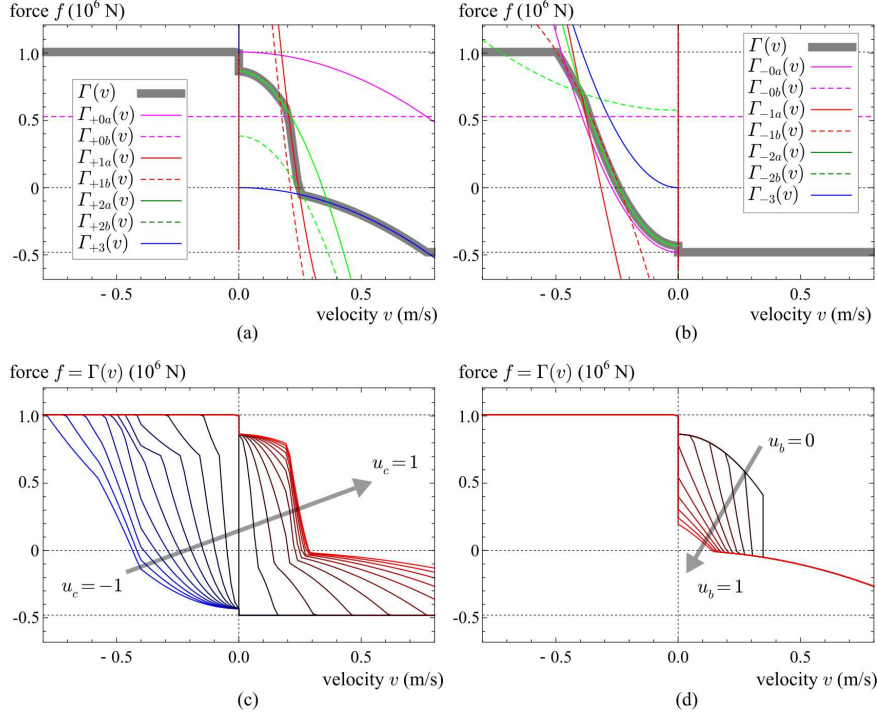


Figure 3: Numerical examples of the quasistatic map $f \in \Gamma(v)$. (a) $u_c = 0.5, u_b = 0.2$; (b) $u_c = -0.5, u_b = 0.2$; (c) $u_c \in [-1, 1], u_b = 0.2$; (d) $u_c = 0.7, u_b \in [0, 1]$. The velocity v is positive when the rod is extending. The force f is positive when the external force is compressive and the actuator force acts to extend the rod.

3.4 Numerical Examples

Some numerical examples are now presented. We consider an asymmetric hydraulic cylinder with the following parameter values:

$$\begin{aligned}
 C_* &= 0.6, \quad a_* = 0.0001 \text{ m}^2, \quad \rho = 850 \text{ kg/m}^3, \\
 A_r &= 0.012 \text{ m}^2, \quad A_h = 0.024 \text{ m}^2, \\
 P_{rM} &= 40 \text{ MPa}, \quad P_{hM} = 42 \text{ MPa}, \quad P_M = 36 \text{ MPa}, \\
 Q &= 500 \text{ L/min} = 0.00833 \text{ m}^3/\text{s}.
 \end{aligned} \tag{46}$$

A common control command $u_c \in [-1, 1]$ is used to set the openings of the main control valves as follows:

$$u_{ph} = u_{tr} = \max(u_c, 0), \quad u_{pr} = u_{th} = \max(-u_c, 0). \tag{47}$$

The opening of the bleed valve was fixed at $u_b = 0.2$ unless otherwise noted.

Results with different values of u_c and u_b are shown in Fig. 3. Fig. 3(a) shows the function Γ and its segments with a positive u_c , while Fig. 3(b) shows those with a negative u_c . They show that $\Gamma(v)$ is always a decreasing function of v and it is set-valued at $v = 0$. Fig. 3(c) shows how the function $\Gamma(v)$ varies according to the change in u_c . It shows that, at a constant external force, the velocity v increases as u_c increases, which is consistent with the behavior of real hydraulic actuator. Fig. 3(d) shows that the velocity v decreases as the bleed valve opening u_b increases. It can be explained by the fact that the oil flow into the actuator decreases as the bleed valve opens.

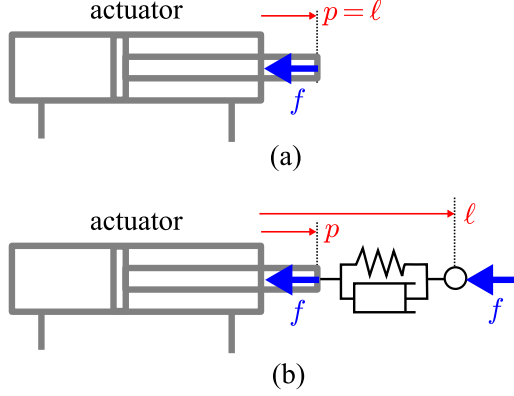


Figure 4: Differential-algebraic relaxation using a virtual viscoelastic element. (a) The original system with the algebraic constraint $f \in \Gamma(\dot{\ell})$. (b) The approximate (relaxed) system with the differential-algebraic constraint (48).

4 Incorporation into Multibody Simulators

4.1 Virtual Viscoelastic Element

The previous section has modeled a hydraulic actuator as a set-valued function Γ from the velocity v to the force f . Because of the set-valuedness, the function Γ is not convenient for the use in simulations. The set-valuedness at $v = 0$ is an important feature that cannot be neglected because the actuator actually stops when the oil flow is blocked by the valves. This section shows an approach to incorporate the set-valued function Γ in multibody simulators.

The quasistatic model presented in the previous section describes the system of Fig. 4(a) as an algebraic constraint $f \in \Gamma(\dot{p})$ where p is the displacement of the actuator rod and $v = \dot{p}$. To deal with the set-valuedness, we consider installing a virtual viscoelastic element connected with the actuator as illustrated in Fig. 4(b). Let ℓ be the total displacement including the viscoelastic element and p be the displacement of the actuator rod. The stretch of the viscoelastic element is $\ell - p$. One can see that, if the viscoelastic element is stiff enough, $p \approx \ell$ is maintained and thus the system of Fig. 4(b) approximates the system of Fig. 4(a). The dynamics of the system of Fig. 4(b) can be described as follows:

$$f = K(p - \ell) + B(\dot{p} - \dot{\ell}) \quad (48a)$$

$$f \in \Gamma(\dot{p}). \quad (48b)$$

Here, K and B are the stiffness and the viscosity of the virtual viscoelastic element. Because there is no inertia between the actuator and the viscoelastic element, f in (48a), determined by the viscoelastic element, is always the same as f in (48b), acting on the actuator. Although some discussions on the choice of K and B will be given in Remark 2, a simple guideline for a better approximation (i.e., $p \approx \ell$) is that the stiffness K should be as high as the simulation is stable, and that the viscosity B should be high enough to damp the oscillation in the relative displacement $p - \ell$. The expression (48) can be seen as a differential-algebraic inclusion (DAI) with respect to p . The quantities ℓ and $\dot{\ell}$ are given as inputs, and \dot{p} and f are determined by the pair (48) of algebraic constraints.

To provide the solution of these algebraic constraints (48), let us consider a function Λ that satisfies the following relation:

$$\beta v + \bar{f} \in \Gamma(v) \iff v = \Lambda(\beta, \bar{f}) \quad (49)$$

where $\beta > 0$. Because $\Gamma(v)$ is a decreasing function of v and $\beta v + \bar{f}$ is a strictly increasing function of v , the algebraic inclusion $\beta v + \bar{f} \in \Gamma(v)$ always has a unique solution with respect to v , and thus $\Lambda(\beta, f)$ is a globally single-valued function. Fortunately, $\Lambda(\beta, \bar{f})$ can be obtained analytically as will be shown in the next Section 4.2. Considering that (48a) is equivalent to $f = B\dot{p} + \bar{f}$ where $\bar{f} = K(p - \ell) - B\dot{\ell}$, the DAI (48) can be equivalently rewritten as follows:

$$\dot{p} = \Lambda(B, K(p - \ell) - B\dot{\ell}) \quad (50a)$$

$$f = K(p - \ell) + B(\dot{p} - \dot{\ell}). \quad (50b)$$

The expression (50) is algebraically equivalent to the expression (48), and can be seen as a closed-form solution of the algebraic problem (48). Moreover, because Λ is a continuous, single-valued function, (50) is only an ordinary differential equation (ODE) representing a first-order system of which the state is p . That is, (50) can be used for simulations combined with common numerical integration schemes.

Another numerical scheme for the DAI (48) can be obtained through the discretization along time. With the implicit (backward) Euler discretization, i.e., $v = \dot{p} \approx (p_k - p_{k-1})/h$ and $\dot{\ell} \approx (\ell_k - \ell_{k-1})/h$, one can discretize (48) as follows:

$$f_k = (B + hK)v + K(p_{k-1} - \ell_k) - B(\ell_k - \ell_{k-1})/h \quad (51a)$$

$$f_k \in \Gamma(v) \quad (51b)$$

$$p_k = p_{k-1} + hv \quad (51c)$$

where k denote the discrete-time index and h denotes the timestep size. The pair of constraints (51a) and (51b) poses an algebraic problem with respect to v and f_k , and the function Λ provides the solutions. That is, we can solve (51) in the following algorithm:

$$\bar{f} := K(p_{k-1} - \ell_k) - B(\ell_k - \ell_{k-1})/h \quad (52a)$$

$$v := \Lambda(B + hK, \bar{f}) \quad (52b)$$

$$p_k := p_{k-1} + hv \quad (52c)$$

$$f_k := \bar{f} + (B + hK)v. \quad (52d)$$

This algorithm accepts the inputs $\{\ell_k, p_{k-1}, \ell_{k-1}\}$ and provides the output f_k , and can be seen as a numerical integration scheme for the DAI (48). In the simulation, the values of $\{p_k, \ell_k\}$ should be stored and used as $\{p_{k-1}, \ell_{k-1}\}$ in the next timestep.

In summary, the original set-valued constraint $f \in \Gamma(\dot{\ell})$ is approximated by the DAI (48), which is implementable as the ODE (50) or the discrete-time algorithm (52). For the implementation, the continuous-time form (50) would be preferred for rather complicated simulations with sophisticated ODE solvers, while the Euler-based discrete-time form (52) would be convenient for rather simple simulations that do not require high accuracy. This approximation scheme, which relaxes a set-valued algebraic constraint by a DAI, is what Kikuuwe [15] has called a *differential algebraic relaxation*. The scheme has been utilized to deal with Coulomb friction in simulators [16, 17, 30, 31] and to implement sliding mode controllers to discrete-time systems [14, 18].

Remark 2. *The choice of K and B can be discussed from two different points of view. On the one hand, if one needs to approximate the ideal situation where the actuator is rigidly connected to external components (such as links of an excavator), the stiffness K should be set as high as the simulation is stable. On the other hand, if one needs to simulate a particular real system that comprises the compliance of the components and the compressibility of the oil, the values of K and B should be chosen so that the simulator's response is close to that of the real system.*

In this case, the values of K and B may be considered as the aggregation of the compliance and damping of the components and the oil. The tuning procedure might be performed by explicitly considering these factors, or on a trial-and-error basis, comparing the data from the simulator and the real system.

4.2 Analytical Form of Function Λ

Now we present an analytical form of $\Lambda(\beta, \bar{f})$, of which the definition has been given only implicitly as in (49). Let v_* denote the solution of $\beta v + \bar{f} = \Gamma_*(v)$ with respect to v where $\Gamma_*(v)$ are those listed in (44). By observing the definitions of $\Gamma_*(v)$ and using Proposition 1 and Proposition 2, we can obtain the followings:

$$v_{+0a} \triangleq \Phi_A(\beta, \bar{f} - F_{hM}, \hat{u}_{tr}^2) \quad (53a)$$

$$v_{+0b} \triangleq (F_{hM} - F_{rM} - \bar{f})/\beta \quad (53b)$$

$$v_{+1a} \triangleq \Phi_B\left(\beta, \bar{f}, \psi(\hat{u}_{ph}, \hat{u}_{tr}), \frac{U_b^2}{A_h^3}, \frac{Q}{A_h}\right) \quad (53c)$$

$$v_{+1b} \triangleq \Phi_B\left(\beta, \bar{f} + F_{rM}, \hat{u}_{ph}^2, \frac{U_b^2}{A_h^3}, \frac{Q}{A_h}\right) \quad (53d)$$

$$v_{+2a} \triangleq \Phi_A(\beta, \bar{f} - A_h P_M, \psi(\hat{u}_{ph}, \hat{u}_{tr})) \quad (53e)$$

$$v_{+2b} \triangleq \Phi_A(\beta, \bar{f} - A_h P_M + F_{rM}, \hat{u}_{ph}^2) \quad (53f)$$

$$v_{+3} \triangleq \Phi_A(\beta, \bar{f}, \hat{u}_{tr}^2) \quad (53g)$$

$$v_{rM} \triangleq (-F_{rM} - \bar{f})/\beta \quad (53h)$$

$$v_{-0a} \triangleq \Phi_A(\beta, \bar{f} + F_{rM}, \hat{u}_{th}^2) \quad (53i)$$

$$v_{-0b} \triangleq (F_{hM} - F_{rM} - \bar{f})/\beta \quad (53j)$$

$$v_{-1a} \triangleq \Phi_B\left(\beta, \bar{f}, \psi(\hat{u}_{pr}, \hat{u}_{th}), \frac{U_b^2}{A_r^3}, -\frac{Q}{A_r}\right) \quad (53k)$$

$$v_{-1b} \triangleq \Phi_B\left(\beta, \bar{f} - F_{hM}, \hat{u}_{pr}^2, \frac{U_b^2}{A_r^3}, -\frac{Q}{A_r}\right) \quad (53l)$$

$$v_{-2a} \triangleq \Phi_A(\beta, \bar{f} + A_r P_M, \psi(\hat{u}_{pr}, \hat{u}_{th})) \quad (53m)$$

$$v_{-2b} \triangleq \Phi_A(\beta, \bar{f} + A_r P_M - F_{hM}, \hat{u}_{pr}^2) \quad (53n)$$

$$v_{-3} \triangleq \Phi_A(\beta, \bar{f}, \hat{u}_{th}^2) \quad (53o)$$

$$v_{hM} \triangleq (F_{hM} - \bar{f})/\beta. \quad (53p)$$

Then, by using Theorem 2 and Theorem 3, the function Λ can be obtained as follows:

$$\Lambda(\beta, \bar{f}) \triangleq \begin{cases} v_{hM} & \text{if } \bar{f} > F_{hM} \wedge \hat{\mathbf{u}} \in (\mathcal{U}_+ \cup \mathcal{U}_0) \\ \Lambda_+(\beta, \bar{f}) & \text{if } \bar{f} < \Gamma_+(0) \wedge \hat{\mathbf{u}} \in \mathcal{U}_+ \\ v_{rM} & \text{if } \bar{f} < -F_{rM} \wedge \hat{\mathbf{u}} \in (\mathcal{U}_- \cup \mathcal{U}_0) \\ \Lambda_-(\beta, \bar{f}) & \text{if } \bar{f} > \Gamma_-(0) \wedge \hat{\mathbf{u}} \in \mathcal{U}_- \\ 0 & \text{if } \Gamma_+(0) \leq \bar{f} \leq \Gamma_-(0) \end{cases} \quad (54a)$$

where

$$\Lambda_+(\beta, \bar{f}) \triangleq \max(\min(\max(v_{+0a}, v_{+0b}), \max(v_{+1a}, v_{+1b}), \max(v_{+2a}, v_{+2b})), v_{+3}, v_{rM}) \quad (54b)$$

$$\Lambda_-(\beta, \bar{f}) \triangleq \min(\max(\min(v_{-0a}, v_{-0b}), \min(v_{-1a}, v_{-1b}), \min(v_{-2a}, v_{-2b})), v_{-3}, v_{hM}). \quad (54c)$$

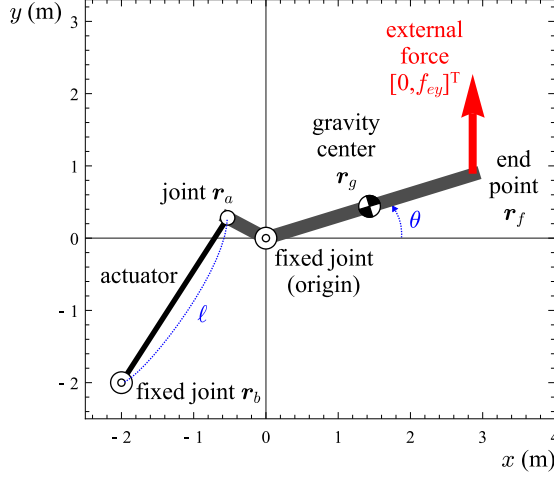


Figure 5: A single-DOF arm driven by a hydraulic actuator.

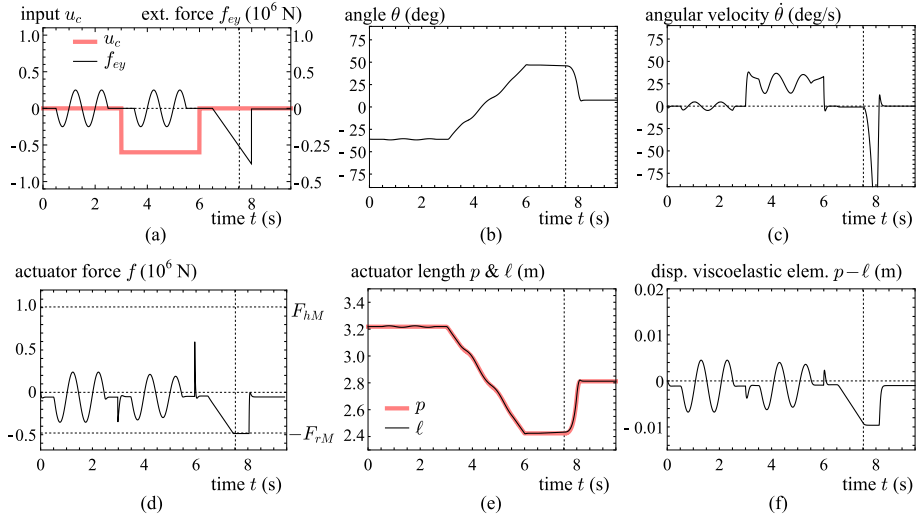


Figure 6: Inputs (a) and results (b)-(f) of the simulation of the system of Fig. 5. The actuator force f is positive when it acts to extend the rod. The actuator force f saturates at $t = 7.404$ s, indicated by the vertical lines.

Here, $\Gamma_+(0)$ and $\Gamma_-(0)$ are those given by (45).

4.3 Numerical Examples

The method is illustrated with a simple dynamics simulation of a single degree-of-freedom (DOF) arm system shown in Fig. 6. The equation of motion is written as follows:

$$(J + ML_g^2)\ddot{\theta} = \mathbf{r}_g \times \begin{bmatrix} 0 \\ -Mg \end{bmatrix} + \mathbf{r}_m \times \left(\frac{\mathbf{r}_m - \mathbf{r}_b}{\|\mathbf{r}_m - \mathbf{r}_b\|} f \right) + \mathbf{r}_f \times \begin{bmatrix} 0 \\ f_{ey} \end{bmatrix} \quad (55)$$

$$\ell = \|\mathbf{r}_m - \mathbf{r}_b\| \quad (56)$$

$$f = K(\ell - p) + B(\dot{\ell} - \dot{p}) \quad (57)$$

$$f \in \Gamma(\dot{p}) \quad (58)$$

where \mathbf{r}_* are those indicated in Fig. 5, which are calculated as follows:

$$\mathbf{r}_g = \begin{bmatrix} L_g \cos \theta \\ L_g \sin \theta \end{bmatrix}, \quad \mathbf{r}_m = \begin{bmatrix} -L_m \cos(\theta - \alpha) \\ -L_m \sin(\theta - \alpha) \end{bmatrix}, \quad \mathbf{r}_f = \begin{bmatrix} L_f \cos \theta \\ L_f \sin \theta \end{bmatrix}. \quad (59)$$

Here, \times stands for a pseudo cross-product of two-dimensional vectors, $[a_1, a_2]^T \times [b_1, b_2]^T = a_1 b_2 - a_2 b_1$. The parameters were set as $L_g = 1.5$ m, $L_m = 0.6$ m, $\alpha = \pi/4$, $L_f = 3$ m, $M = 2000$ kg, and $J = 5000$ kg·m². The parameters for the virtual viscoelastic elements were chosen as $K = 5 \times 10^7$ N/m and $B = 2.5 \times 10^6$ N/m, which as high as the simulation was numerically stable. The parameters of the actuator were set the same as in Section 3.4. The openings of the main control valves were given by (47) with the command $u_c \in [-1, 1]$, and the bleed valve opening was set as $u_b = 0.3$. The timestep size was set as $h = 0.001$ s. At every timestep, the following procedure was performed:

1. Calculate \mathbf{r}_g , \mathbf{r}_m , and \mathbf{r}_f according to (59) with θ determined by the previous timestep, and calculate ℓ according to (56).
2. Calculate f and update p according to the algorithm (52) with the command u_c and the obtained ℓ .
3. Update θ and $\dot{\theta}$ according to the equation of motion (55) with the inputs f and f_{ey} .

The initial value of p was set equal to that of ℓ .

In the simulation, the command u_c and f_{ey} were given as indicated in Fig. 6(a). The results are shown in Figs. 6(b)-(f). From $t = 0$ s to 3 s, the valves are closed and thus the arm holds its angle even under the fluctuating external force f_{ey} . From $t = 3$ s to 6 s, the arm moves up due the negative u_c (to retract the rod). Fig. 6(c) shows that the velocity is more fluctuating in this period than when $u_c = 0$. This behavior is consistent with the fact that hydraulic actuators become more compliant to external forces when the valves are open and the oil is permitted to flow. After $t = 6$ s, the valves are closed again, and the increasing external force does not cause movement of the arm until $t = 7.404$ s, with the increasing actuator force f balancing the external force. At $t = 7.404$ s, the actuator force f reaches the value of $-F_{rM}$ at which the rod-side relief valve opens, and the arm starts to move down. In the whole period, the displacement $p - \ell$ of the viscoelastic element is maintained small (less than a few centimeters), exhibiting the validity of the relaxation scheme introduced in Section 4.1. In conclusion, the results support the usefulness of the proposed model and the relaxation scheme for reproducing qualitative features of hydraulic actuators.

Remark 3. *The transient responses seen in Fig. 6, such as the spikes in the actuator force f at $t \approx 3$ s and $t \approx 6$ s, are determined by the values of K and B . As discussed in Remark 2, one needs to tune the values of K and B so that the simulator exhibits similar responses to the real system.*

5 Extension 1: Regeneration Circuit

5.1 Quasistatic Model

In some practical applications, the circuit of Fig. 1 includes an additional pathway from the rod-side chamber to the head-side chamber to make the extending movement faster. This section considers the circuit of Fig. 7, which is an extension of the circuit of Fig. 1. We assume that the regeneration pipeline has a valve that flows only from the head side to the rod side, and assume that the cross-sectional areas of the cylinder satisfy

$$A_h \geq A_r. \quad (60)$$

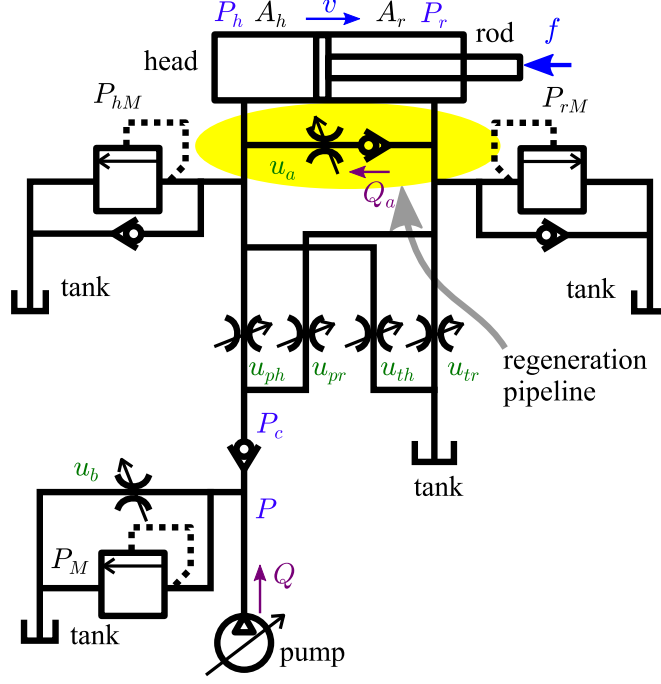


Figure 7: Regeneration pipeline added to the circuit of Fig. 1.

There must be some cylinders that do not satisfy (60), but the removal of this assumption is left for future study. Let a_a is the maximum opening area (m^2) of the regeneration valve, and let $u_a \in [0, 1]$ be the dimensionless input value, which is the ratio of the valve opening area to its maximum value a_a . Then, the flowrate of the oil through the regeneration pipeline is written as follows:

$$Q_a = c_a u_a \max(\mathcal{R}(F_r/A_r - F_h/A_h, 0)) \quad (61)$$

where $c_a \triangleq C_a a_a \sqrt{2/\rho}$ where C_a is the discharge coefficient of the regeneration valve, typically around 0.6 or 0.7.

With this regeneration pipeline and its flowrate Q_a , (27) is extended into the following:

$$-v + \hat{u}_{ph} \mathcal{R}(A_h P_c - F_h) - \hat{u}_{th} \mathcal{R}(F_h) \in \mathcal{N}_{[0, F_{hM}]}(F_h) - Q_a/A_h \quad (62a)$$

$$v + \hat{u}_{pr} \mathcal{R}(A_r P_c - F_r) - \hat{u}_{tr} \mathcal{R}(F_r) \in \mathcal{N}_{[0, F_{rM}]}(F_r) + Q_a/A_r \quad (62b)$$

$$A_h \hat{u}_{ph} \mathcal{R}(A_h P_c - F_h) + A_r \hat{u}_{pr} \mathcal{R}(A_r P_c - F_r) \in \mathcal{N}_{(-\infty, P_c]}(P) \quad (62c)$$

$$Q \in U_b \mathcal{R}(P) + A_h \hat{u}_{ph} \mathcal{R}(A_h P_c - F_h) + A_r \hat{u}_{pr} \mathcal{R}(A_r P_c - F_r) + \mathcal{N}_{(-\infty, P_M]}(P) \quad (62d)$$

$$f = F_h - F_r. \quad (62e)$$

With $Q_a = 0$, which results from $u_a = 0$, (62) reduces to (27). Let us assume that u_a is set positive only when $\hat{\mathbf{u}} \in \mathbf{U}_+$ because it is the case in many practical hydraulic circuits. In addition, we assume that $u_{tr} > 0$ for the simplicity. Under these conditions, (62) and (61) reduce to the following:

$$\hat{A}v_a - v + \hat{u}_{ph} \mathcal{R}(A_h P_c - F_h) \in \mathcal{N}_{[0, F_{hM}]}(F_h) \quad (63a)$$

$$v - v_a - \hat{u}_{tr} \mathcal{R}(F_r) \in \mathcal{N}_{[0, F_{rM}]}(F_r) \quad (63b)$$

$$A_h \hat{u}_{ph} \mathcal{R}(A_h P_c - F_h) \in \mathcal{N}_{(-\infty, P_c]}(P) \quad (63c)$$

$$Q \in U_b \mathcal{R}(P) + A_h \hat{u}_{ph} \mathcal{R}(A_h P_c - F_h) + \mathcal{N}_{(-\infty, P_M]}(P) \quad (63d)$$

$$f = F_h - F_r \quad (63e)$$

$$v_a = \hat{u}_a \max(\mathcal{R}(F_r - \hat{A}F_h, 0)) \quad (63f)$$

where $v_a \triangleq Q_a/A_r$, $\hat{u}_a \triangleq c_a u_a/A_r^{3/2}$ and $\hat{A} = A_r/A_h$.

By carefully observing (63), one can see that $v_a > 0$ implies $F_r > 0$ from (63f), which implies $v_a \leq v$ from (63b). Its contraposition is that $v_a > v$ implies $v_a = 0$. Therefore, (63) imposes the condition $0 \leq v_a \leq \max(0, v)$. When $v < 0$, the solutions are obviously $v_a = 0$ and $f \in \Gamma(v)$. Therefore, hereafter we consider only the case $v > 0$, in which $v_a > 0$ may take place. By using the functions defined in (41) and (42), the first four equations of (63) can be rewritten as $F_h \in \Gamma_h(v - \hat{A}v_a)$ and $F_r \in \Gamma_r(v - v_a)$ with P_c and P being eliminated. Considering the definitions of Γ_h and Γ_r , because of the conditions $v - v_a \geq 0$, $v > 0$, $u_{tr} > 0$ and $\hat{A} \in (0, 1)$, Γ_h and Γ_r are always single-valued and thus can be replaced by Γ_{h+} and Γ_{r+} , respectively. Therefore, (63) can be rewritten as follows:

$$\Xi_v(v, v_a) \in -\mathcal{N}_{[0, \infty)}(v_a) \quad (64a)$$

$$f = \Gamma_{h+}(v - \hat{A}v_a) - \Gamma_r(v - v_a) \quad (64b)$$

where

$$\Xi_v(v, v_a) \triangleq \mathcal{S}(v_a) - \hat{u}_a^2(\Gamma_{r+}(v - v_a) - \hat{A}\Gamma_{h+}(v - \hat{A}v_a)). \quad (65)$$

This expression can be seen as an algebraic problem regarding $\{f, v_a\}$ with a given v .

The function $\Xi_v(v, v_a)$ is an increasing function of v_a and it satisfies $\Xi_v(v, v) > 0$ because of $\Gamma_{r+}(0) = 0$. With the algebraic constraint (64a), $\Xi_v(v, 0) \geq 0$ implies that the solution is $v_a = 0$. Meanwhile, if $\Xi_v(v, 0) < 0$, the solution can be found within the region $v_a \in [0, v]$ by simple root-finding schemes. Once the solution v_a is obtained, f is obtained by (64b).

In conclusions, f and v_a satisfying (64) are obtained by the following functions:

$$f \in \Gamma_{\text{reg}}(v) \triangleq \begin{cases} \Gamma(v) & \text{if } u_a = 0 \vee \hat{u} \notin \mathcal{U}_+ \vee v \leq 0 \vee \Xi_v(v, 0) \geq 0 \\ \Gamma_{h+}(v - \hat{A}\hat{v}_a(v)) - \Gamma_{r+}(v - \hat{v}_a(v)) & \text{otherwise} \end{cases} \quad (66)$$

$$v_a = \hat{v}_a(v) \triangleq \begin{cases} 0 & \text{if } u_a = 0 \vee \hat{u} \notin \mathcal{U}_+ \vee v \leq 0 \vee \Xi_v(v, 0) \geq 0 \\ \text{FindRoot}(\Xi_v(v, \bullet), [0, v]) & \text{otherwise.} \end{cases} \quad (67)$$

Here, ‘‘FindRoot’’ is a function that finds a root of the argument function within the range specified by the second argument. This computation can be performed with a common iterative method, such as the Bisection method or the false position method, because $\Xi_v(v, v_a)$ is continuous and monotonic. It may also be possible to find analytical methods because $\Xi_v(v, v_a)$ is only a piece-wise parabolic function. The function Γ_{reg} can be seen as an extension of the quasistatic map Γ given in Section 3.3.

Some numerical examples of Γ_{reg} and \hat{v}_a are presented in Fig. 8. It can be seen that, as u_a increases (i.e., as the regeneration valve opens), the extending velocity of the rod tends to increase especially in the region $f < 0$, i.e., under stretching external forces. It can also be seen that the flowrate Q_a through the regeneration valve increases as u_a and v increase. These features are consistent with those of actual hydraulic actuators.

5.2 Incorporation into Simulators

As has been discussed in Section 4, multibody simulations involving the quasistatic map $f \in \Gamma(v)$ require its correspondent Λ defined by (49). In the same manner, now we consider obtaining the function Λ_{reg} that satisfies the following:

$$\beta v + \bar{f} \in \Gamma_{\text{reg}}(v) \iff v = \Lambda_{\text{reg}}(\beta, \bar{f}). \quad (68)$$

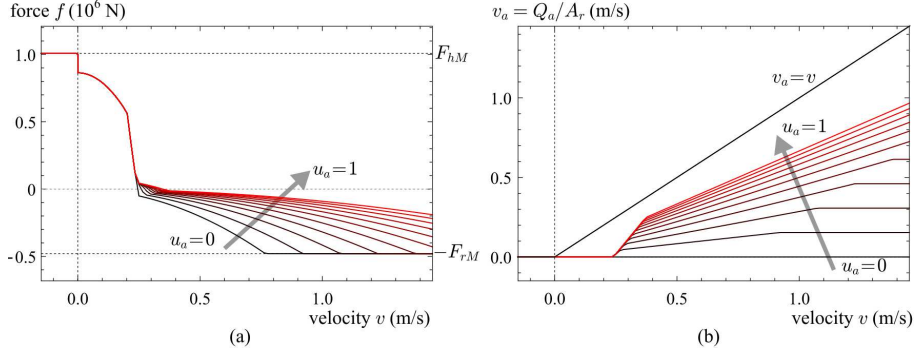


Figure 8: Numerical examples of the quasistatic map $f \in \Gamma_{\text{reg}}(v)$ and $v_a = \hat{v}_a(v)$ of the circuit of Fig. 7, which includes a regeneration pipeline. The parameters are set the same as in Section 3.4 except $C_a = 0.6$ and $a_a = 0.0001 \text{ m}^2$. The valve openings are set as $u_c = 0.5$ (see (47)) and $u_b = 0.2$.

To this end, we consider the algebraic problem (64) with f being replaced by $f = \beta v + \bar{f}$ and v being treated as an unknown, which is written as follows:

$$\Xi_v(v, v_a) \in -\mathcal{N}_{[0, \infty)}(v_a) \quad (69a)$$

$$\Xi_f(v, v_a) = 0 \quad (69b)$$

where

$$\Xi_f(v, v_a) \triangleq \beta v + \bar{f} - \Gamma_{h+}(v - \hat{A}v_a) + \Gamma_{r+}(v - v_a). \quad (70)$$

The expression (69) is an algebraic problem regarding $\{v, v_a\}$ with a given \bar{f} .

The problem (69) is illustrated in Fig. 9, in which the sets of $\{v, v_a\}$ satisfying (69a) and (69b) are shown as curves. The functions $\Xi_v(v_a, v)$ and $\Xi_f(v_a, v)$ are increasing with respect to v_a and v , respectively. The region $0 \leq v_a < v$ should be searched for the solution $\{v, v_a\}$. Because $f = \beta v + \bar{f} \in [-F_{rM}, F_{hM}]$, one can see that the solution exists in the region $(-F_{rM} - \bar{f})/\beta < v < (F_{hM} - \bar{f})/\beta$. In addition, the solution v of $\Xi_f(v, v_a) = 0$ with $v_a > 0$ is larger than $\Lambda(\beta, \bar{f})$, which is the solution with $v_a = 0$. Therefore, the trapezoidal area in Fig. 9 is the region that must be searched for the solution $\{v, v_a\}$.

As shown in Fig. 9(a), if $\{\Lambda(\beta, \bar{f}), 0\}$, which is an analytically obtained initial guess, resides in the region $\Xi_v(v, v_a) < 0$, it is the solution of the problem (69). Otherwise, the solution can be searched for iteratively, as illustrated in Fig 9(b), by alternately searching in v_a and v -directions from the initial guess $\{\Lambda(\beta, \bar{f}), 0\}$. The following is an algorithm to obtain the solution:

$$\text{Function } \Lambda_{\text{reg}}(\beta, \bar{f}) \quad (71a)$$

$$v := \Lambda(\beta, \bar{f}) \quad (71b)$$

$$\text{If } u_a > 0 \wedge \hat{\mathbf{u}} \in \mathbf{U}_+ \wedge v > 0 \wedge \Xi_v(v, 0) < 0 \text{ Then} \quad (71c)$$

$$v_a := 0 \quad (71d)$$

$$\text{Loop} \quad (71e)$$

$$v_a := \text{FindRoot}(\Xi_v(v, \bullet), [v_a, v]) \quad (71f)$$

$$\text{If } |\Xi_f(v, v_a)| < \varepsilon_f \text{ Exit Loop} \quad (71g)$$

$$v := \text{FindRoot}(\Xi_f(\bullet, v_a), [v, (F_{hM} - \bar{f})/\beta]) \quad (71h)$$

$$\text{If } |\Xi_v(v, v_a)| < \varepsilon_v \text{ Exit Loop} \quad (71i)$$

$$\text{While} \quad (71j)$$

$$\text{End If} \quad (71k)$$

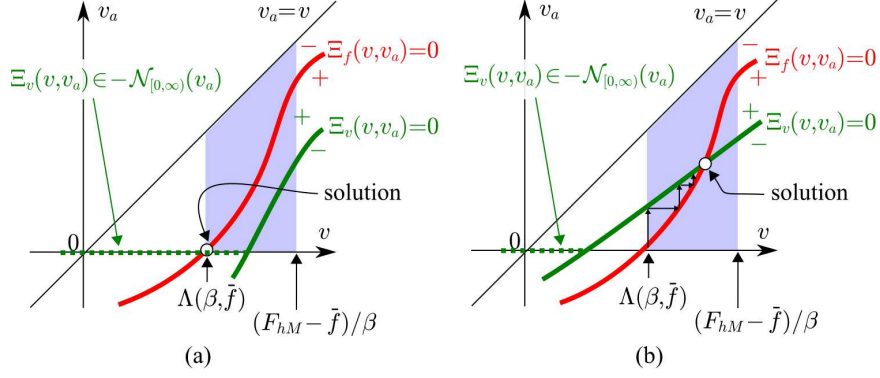


Figure 9: Solution of the problem (69) in (a) the case of $\Xi_v(\Lambda(\beta, \bar{f}), 0) \geq 0$, where $\{v, v_a\} = \{\Lambda(\beta, \bar{f}), 0\}$ is the solution, and (b) the case of $\Xi_v(\Lambda(\beta, \bar{f}), 0) < 0$, where iterative computation is needed.

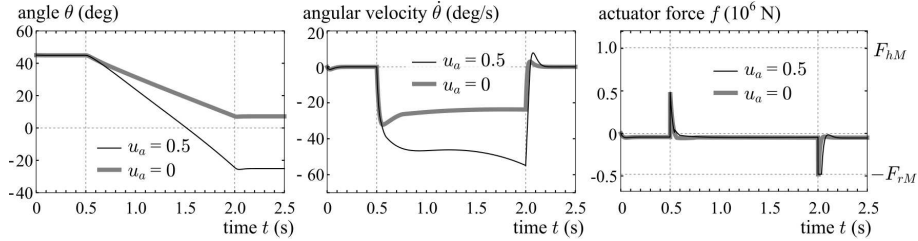


Figure 10: Simulation results of the system of Fig. 5 with the regeneration valve being open ($u_a = 0.5$) and closed ($u_a = 0$).

Return v . (711)

Here, ε_f and ε_v are very small positive numbers. This algorithm can be seen as an extension of $\Lambda(\beta, \bar{f})$ given in Section 4.2. As is the case with Γ_{reg} , the computation of “FindRoot” can be performed with common iterative solvers. Some analytical methods may be found because Ξ_f is also a piece-wise parabolic function.

Some simulations were performed with the same arm system as in Section 4.3 and Fig. 5. The arm was moved down from $\theta = 30$ deg for 1.5 s with the command $u_c = 0.5$ with the regeneration valve being open ($u_a = 0.5$) and closed ($u_a = 0$). The results are shown in Fig. 10. It shows that $u_a > 0$ realizes a faster extending motion, which is consistent with the effects of actual regeneration circuits. In addition, it can be seen that the impulsive actuator force at the beginning of the motion (around $t = 0.5$ s) is smaller with $u_a > 0$. It can be explained by the fact that the open regeneration valve allows more flow of the oil, resulting in a softer response. The impulses at the end of the movement (around $t = 2$ s) should not be directly compared because the angle and the velocity at this time are quite different between the two conditions.

6 Extension 2: Multiple Actuators Driven by One Pump

6.1 Quasistatic Model

In some excavators, more than one actuators are actuated by a single pump as illustrated in Fig. 11. In such a circuit, the behaviors of the actuators influence each other, e.g., the movement of one actuator may decrease the supplied flowrate to other actuators. This section presents an extension of the quasistatic model to deal with such systems.

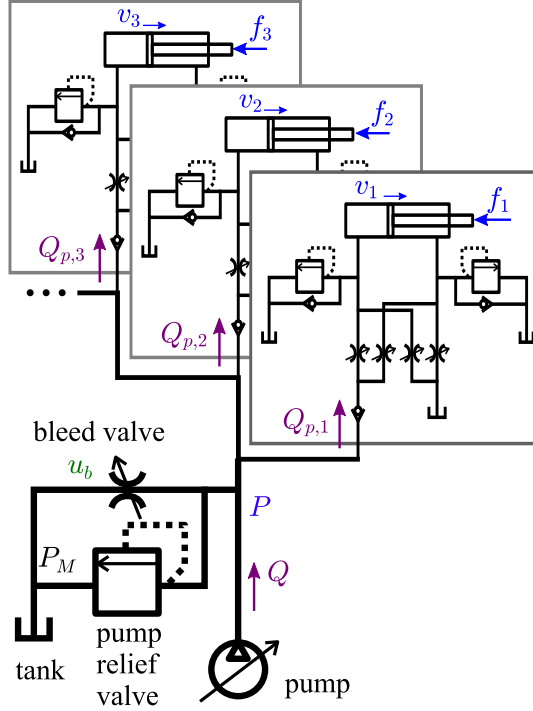


Figure 11: Multiple actuators driven by one pump.

In circuits like Fig. 11, the actuators are connected to a junction at which the pressure is P , and the total supplied flowrate Q from the pump is equal to the sum of the supplied flowrates to all actuators plus that discharged through the bleed valve and the pump relief valve. On the other hand, the actuator model developed in Section 3.3 assumes that the supplied flowrate Q from the pump is the input to be given. Therefore, one can see that it is convenient to have a modified version of the quasistatic map Γ of which the input is the pressure P instead of the flowrate Q .

With a close look at the definition (44) of the function Γ in Section 3.3, one can see that a P -input version of the quasistatic map Γ can be obtained by replacing P_m by P and removing the segments depending on Q . Specifically, the modified version $\hat{\Gamma}(P, v)$, which maps the velocity v to the force f of an actuator depending on P , can be given as follows:

$$f \in \hat{\Gamma}(P, v) \triangleq \text{gsign}(\hat{\Gamma}_-(P, v), v, \hat{\Gamma}_+(P, v)) \quad (72a)$$

where

$$\hat{\Gamma}_+(P, v) \triangleq \max(\min(\max(\Gamma_{+0a}(v), \Gamma_{+0b}(v)), \max(\hat{\Gamma}_{+2a}(P, v), \hat{\Gamma}_{+2b}(P, v))), \Gamma_{+3}(v), -F_{rM}) \quad (72b)$$

$$\hat{\Gamma}_-(P, v) \triangleq \min(\max(\min(\Gamma_{-0a}(v), \Gamma_{-0b}(v)), \min(\hat{\Gamma}_{-2a}(P, v), \hat{\Gamma}_{-2b}(P, v))), \Gamma_{-3}(v), F_{hM}) \quad (72c)$$

$$\hat{\Gamma}_{+2a}(P, v) \triangleq A_h P - \frac{\mathcal{S}(v)}{\hat{u}_{ph}^2} - \frac{\mathcal{S}(v)}{\hat{u}_{tr}^2} \quad (72d)$$

$$\hat{\Gamma}_{+2b}(P, v) \triangleq A_h P - \frac{\mathcal{S}(v)}{\hat{u}_{ph}^2} - F_{rM} \quad (72e)$$

$$\hat{\Gamma}_{-2a}(P, v) \triangleq -A_r P - \frac{\mathcal{S}(v)}{\hat{u}_{pr}^2} - \frac{\mathcal{S}(v)}{\hat{u}_{th}^2} \quad (72f)$$

$$\widehat{\Gamma}_{-2b}(P, v) \triangleq -A_r P - \frac{\mathcal{S}(v)}{\hat{u}_{pr}^2} + F_{hM}. \quad (72g)$$

Here, the functions without hats are those defined in (44). In the same manner as (45), we also have the following:

$$\widehat{\Gamma}_+(P, 0) = \widehat{\Gamma}_{h+}(P, 0) - \widehat{\Gamma}_{r+}(P, 0), \quad \widehat{\Gamma}_-(P, 0) = \widehat{\Gamma}_{h-}(P, 0) - \widehat{\Gamma}_{r-}(P, 0) \quad (73a)$$

where

$$\widehat{\Gamma}_{h+}(P, 0) = \begin{cases} \min(F_{hM}, A_h P) & \text{if } \hat{u}_{ph} > 0 \\ 0 & \text{if } \hat{u}_{ph} = 0 \end{cases} \quad (73b)$$

$$\widehat{\Gamma}_{r+}(P, 0) = \begin{cases} 0 & \text{if } \hat{u}_{tr} > 0 \\ F_{rM} & \text{if } \hat{u}_{tr} = 0 \end{cases} \quad (73c)$$

$$\widehat{\Gamma}_{h-}(P, 0) = \begin{cases} 0 & \text{if } \hat{u}_{th} > 0 \\ F_{hM} & \text{if } \hat{u}_{th} = 0 \end{cases} \quad (73d)$$

$$\widehat{\Gamma}_{r-}(P, 0) = \begin{cases} \min(F_{rM}, A_r P) & \text{if } \hat{u}_{pr} > 0 \\ 0 & \text{if } \hat{u}_{pr} = 0. \end{cases} \quad (73e)$$

The flowrate Q_p into an actuator is determined by the pressure P at the junction and the pressure P_h or P_r of the chamber connected to the pump, specifically, as follows:

$$Q_p = A_h \hat{u}_{ph} \max(\mathcal{R}(A_h P - F_h), 0) + A_r \hat{u}_{pr} \max(\mathcal{R}(A_r P - F_r), 0). \quad (74)$$

If $\hat{\mathbf{u}} \in \mathbf{U}_+$, we have $F_h = f + F_r$ and $F_r = \text{proj}_{[0, F_{rM}]}(\mathcal{S}(v)/\hat{u}_{tr}^2)$. If $\hat{\mathbf{u}} \in \mathbf{U}_-$, we have $F_h = \text{proj}_{[0, F_{hM}]}(\mathcal{S}(v)/\hat{u}_{th}^2)$ and $F_r = F_h - f$. Therefore, Q_p is obtained as follows:

$$Q_p = \widehat{Q}_p(P, v, \widehat{\Gamma}(P, v)) \quad (75)$$

where

$$\widehat{Q}_p(P, v, \widehat{\Gamma}(P, v)) \triangleq \begin{cases} A_h \hat{u}_{ph} \max(\mathcal{R}(A_h P - \text{proj}_{[0, F_{rM}]}(\mathcal{S}(v)/\hat{u}_{tr}^2) - f), 0) & \text{if } \hat{\mathbf{u}} \in \mathbf{U}_+ \\ 0 & \text{if } \hat{\mathbf{u}} \in \mathbf{U}_0 \\ A_r \hat{u}_{pr} \max(\mathcal{R}(A_r P - \text{proj}_{[0, F_{hM}]}(-\mathcal{S}(v)/\hat{u}_{th}^2) + f), 0) & \text{if } \hat{\mathbf{u}} \in \mathbf{U}_-. \end{cases} \quad (76)$$

The function $\widehat{\Gamma}$ appearing in (75) may be set-valued at $v = 0$, but a careful observation of its limits of both sides of zero shows that $\widehat{Q}_p(P, 0, \widehat{\Gamma}(P, 0)) = 0$, single-valued, under all three conditions, \mathbf{U}_+ , \mathbf{U}_0 and \mathbf{U}_- .

By using the function \widehat{Q}_p , the algebraic constraint between the total flowrate Q from the pump and the pressure P can be described as follows:

$$\Xi_P(P) \in \mathcal{N}_{(-\infty, P_M]}(P) \quad (77a)$$

where

$$\Xi_P(P) \triangleq Q - U_b \mathcal{R}(P) - \sum_{j=1}^N \widehat{Q}_{p,j}(P, v_j, \widehat{\Gamma}_j(P, v_j)). \quad (77b)$$

Here, the symbols with the subscript j stand for those associated with the j th actuator, and N denotes the number of actuators. The value of $\Xi_P(P)$ can be interpreted as the flowrate from the pump relief valve (see Fig. 11), which is the difference between the oil supply from the pump and the sum of the oil supplies to all actuators plus that to the bleed valve. As long as $P < P_M$,

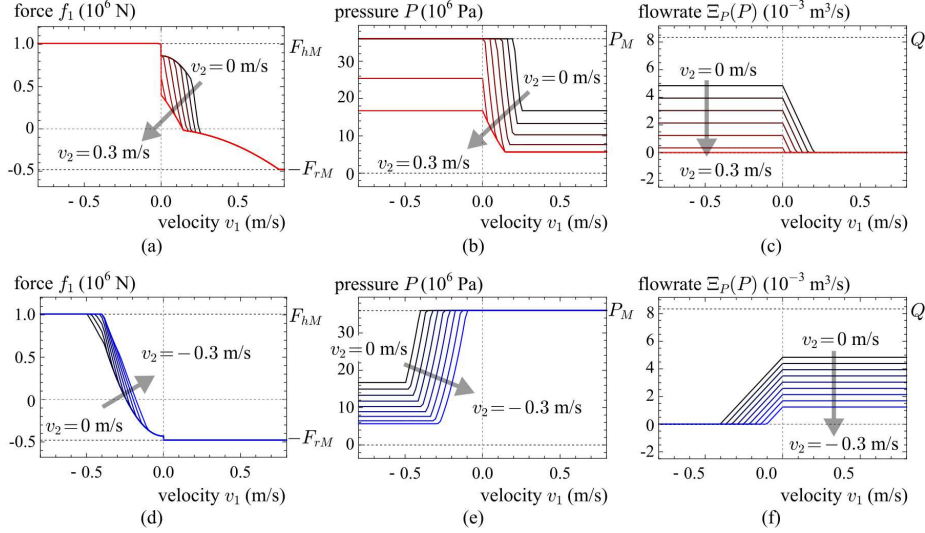


Figure 12: Numerical examples regarding the quasistatic map $[f_1, f_2]^T \in \Gamma_{\text{mul}}([v_1, v_2]^T)$ of a circuit including two identical actuators driven by a single pump. Positive commands $u_{c,1} = u_{c,2} = 0.5$ are given in (a)-(c) and negative commands $u_{c,1} = u_{c,2} = -0.5$ are given in (d)-(f) (see (47)).

(77a) reduces to $\Xi_P(P) = 0$, which means that the pump relief valve is closed. When $P = P_M$, (77a) reduces to $\Xi_P(P) \geq 0$, which means that the oil is discharged from the pump relief valve, of which the pressure limit is P_M . The pressure P can be found by solving the algebraic problem (77) as follows:

$$P = \begin{cases} P_M & \text{if } \Xi_P(P_M) \geq 0 \\ \text{FindRoot}(\Xi_P(\bullet), [0, P_M]) & \text{otherwise.} \end{cases} \quad (78)$$

This “FindRoot” is also easy because of the monotonicity of the function Ξ_P .

By using the value of P obtained by (78), the quasistatic relation between the forces $\mathbf{f} = [f_1, \dots, f_N]^T$ and the velocities $\mathbf{v} = [v_1, \dots, v_N]^T$ of N actuators are written in the following form:

$$\mathbf{f} \in \Gamma_{\text{mul}}(\mathbf{v}) \triangleq \left[\hat{\Gamma}_1(P, v_1), \dots, \hat{\Gamma}_N(P, v_N) \right]^T \quad (79)$$

where P is the one obtained by (78).

Some numerical examples are shown in Fig. 12. In these examples, two identical actuators 1 and 2 share a single pump. The parameters of the actuators are the same as those in Section 3.4. The force f_1 obtained by the map $[f_1, f_2]^T \in \Gamma_{\text{mul}}([v_1, v_2]^T)$ according to the variable v_1 and some fixed values of v_2 are shown in Figs. 12(a) and (d). Intermediate values P and $\Xi_P(P)$, which are the immediate output of the root finding in (78), are presented in Figs. 12(b)(c) and (e)(f). It can be seen that an increased speed v_2 of the actuator 2 results in a decreased speed v_1 of the actuator 1, a decreased pressure P at the junction, and a decreased flowrate $\Xi_P(P)$ from the pump relief valve, which are consistent with what can happen in real hydraulic circuits.

6.2 Incorporation into Simulators

In the same way as in Section 4 and in Section 5.2, the application of the quasistatic map Γ_{mul} to multibody simulations requires a map Λ_{mul} that satisfies the following relation:

$$\text{diag}[\beta]\mathbf{v} + \bar{\mathbf{f}} \in \Gamma_{\text{mul}}(\mathbf{v}) \iff \mathbf{v} \in \Lambda_{\text{mul}}(\beta, \bar{\mathbf{f}}) \quad (80)$$

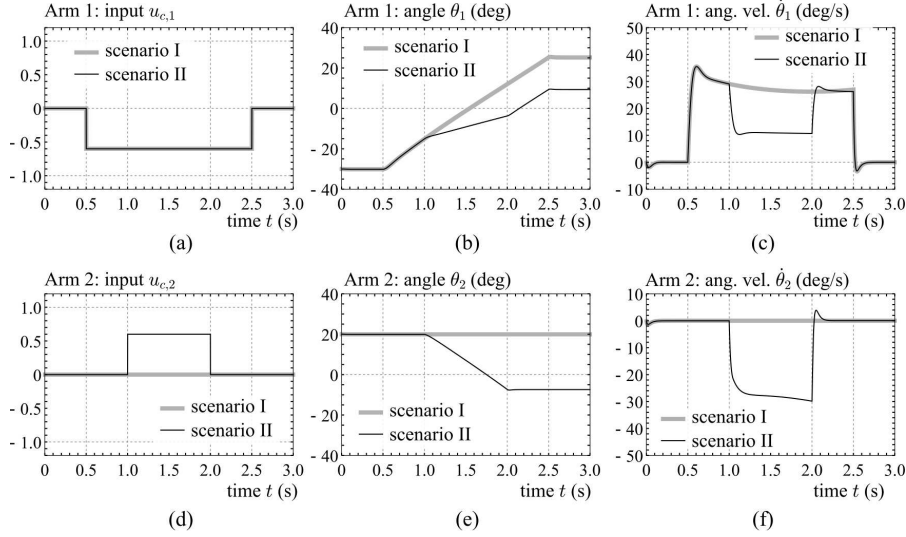


Figure 13: Simulation results of two arms identical to the one in Fig. 5 driven by a single pump. No external forces were applied to either arm. The command $u_{c,1}$ sent to the arm 1 was the same between the two scenarios, while the arm 2 was actuated only in Scenario II.

where β , \mathbf{v} and $\bar{\mathbf{f}}$ are N -dimensional vectors and the elements of β are all positive. The structure (79) of Γ_{mul} suggests that Λ_{mul} has the following structure:

$$\Lambda_{\text{mul}}(\beta, \bar{\mathbf{f}}) = [\hat{\Lambda}_1(P, \beta_1, \bar{f}_1), \dots, \hat{\Lambda}_N(P, \beta_N, \bar{f}_N)]^T \quad (81)$$

where $\hat{\Lambda}_j(P, \beta_j, \bar{f}_j)$ are those that satisfy the following:

$$\beta_j v_j + \bar{f}_j \in \hat{\Gamma}_j(P, v_j) \iff v_j \in \hat{\Lambda}(P, \beta_j, \bar{f}). \quad (82)$$

Recalling that Λ is obtained as (53) and (54), one can obtain $\hat{\Lambda}_j$ as follows:

$$\hat{\Lambda}(P, \beta, \bar{f}) = \begin{cases} v_{hM} & \text{if } \bar{f} \geq F_{hM} \wedge \mathbf{u} \in \mathcal{U}_+ \\ \max(\min(\max(v_{+0a}, v_{+0b}), \max(\hat{v}_{+2a}, \hat{v}_{+2b})), v_{+3}, v_{rM}) & \text{if } \bar{f} \leq \hat{\Gamma}_+(P, 0) \wedge \mathbf{u} \in \mathcal{U}_+ \\ v_{rM} & \text{if } \bar{f} \leq -F_{rM} \wedge \mathbf{u} \in \mathcal{U}_- \\ \min(\max(\min(v_{-0a}, v_{-0b}), \min(\hat{v}_{-2a}, \hat{v}_{-2b})), v_{-3}, v_{hM}) & \text{if } \bar{f} \geq \hat{\Gamma}_-(P, 0) \wedge \mathbf{u} \in \mathcal{U}_- \\ 0 & \text{if } \hat{\Gamma}_+(P, 0) < \bar{f} < \hat{\Gamma}_-(P, 0) \end{cases} \quad (83a)$$

where

$$\hat{v}_{+2a} \triangleq \Phi_A(\beta, \bar{f} - A_h P, \psi(\hat{u}_{ph}, \hat{u}_{tr})) \quad (83b)$$

$$\hat{v}_{+2b} \triangleq \Phi_A(\beta, \bar{f} - A_h P + F_{rM}, \hat{u}_{ph}^2) \quad (83c)$$

$$\hat{v}_{-2a} \triangleq \Phi_A(\beta, \bar{f} + A_r P, \psi(\hat{u}_{pr}, \hat{u}_{th})) \quad (83d)$$

$$\hat{v}_{-2b} \triangleq \Phi_A(\beta, \bar{f} + A_r P - F_{hM}, \hat{u}_{pr}^2). \quad (83e)$$

Here, the subscript j denoting the actuator indices are omitted and the symbols without hats are those defined in (53).

In the expression (81), the pressure P can be obtained in the same line of thought as in Section 6.1, but the problem (77) needs to be modified because v_j are unknowns. Considering that $\bar{\mathbf{f}}$ is given, the problem is redefined as

$$\Xi_{P\Lambda}(P) \in \mathcal{N}_{(-\infty, P_M]}(P) \quad (84a)$$

where

$$\Xi_{P\Lambda}(P) \triangleq Q - U_b \mathcal{R}(P) - \sum_{j=1}^N \widehat{Q}_{p,j}(P, \widehat{\Lambda}_j(\beta_j, \bar{\mathbf{f}}_j), \bar{\mathbf{f}}_j + \beta_j \widehat{\Lambda}_j(\beta_j, \bar{\mathbf{f}}_j)). \quad (84b)$$

The solution P of the problem (84) can be written as follows:

$$P = \begin{cases} P_M & \text{if } \Xi_{P\Lambda}(P_M) \geq 0 \\ \text{FindRoot}(\Xi_{P\Lambda}(\bullet), [0, P_M]) & \text{otherwise.} \end{cases} \quad (85)$$

In conclusion, the function $\mathbf{\Lambda}_{\text{mul}}$ satisfying (80) is obtained as (81) in which $\widehat{\Lambda}_j$ are those defined by (83) and P is replaced by (85).

Some simulations were performed with a system composed of two arms identical to the one in Fig. 5 connected with a single pump. It was implemented with the function $\mathbf{\Lambda}_{\text{mul}}$ with $N = 2$. The parameters of the arms were set the same as in Section 4.3, and the parameters of the actuators and the circuit were set the same as in Section 6.1. No external forces were applied to either arm. The results are shown in Fig. 13. The initial postures of the arms 1 and 2 were set as $\theta = -30$ deg and $\theta = 20$ deg, respectively. In the first scenario, the arm 1 was driven upward by the command $u_{c,1} = -0.6$ from $t = 0.5$ s to 2.5 s. while the arm 2 was not driven. In the second scenario, the command to the arm 1 was the same as that in the first scenario, the arm 2 was driven downward from $t = 1$ s to 2 s. As can be seen in Figs. 13(b) and (c), the actuation of the arm 2 affected the motion of the arm 1, i.e., the arm 1 was decelerated when the arm 2 was actuated. It can be explained by the effect of the arm 2, which suctioned the oil when actuated, causing the shortage of the oil flow into the arm 1.

7 Conclusions

This article has presented a quasistatic model of a hydraulic actuator driven by a four-valve independent metering circuit. The presented model is described as a nonsmooth map between the velocity and the force. The model is derived from the algebraic constraint between the flowrate and the pressure at every valve in the circuit in the steady state. This article also presents an approach to incorporate the quasistatic model into the multibody dynamics simulators, in which the hydraulic model is connected to rigid bodies through virtual viscoelastic elements. In addition, the proposed model is extended to include a regeneration pipeline and to deal with a collection of actuators driven by a single pump.

In multibody simulations employing the presented quasistatic model, the transient responses are determined by the virtual viscoelastic elements, which are parameterized by the stiffness K and the viscosity B . In reality, transient responses are governed by many factors such as the compressibility of the oil, the inertia of the actuator and the oil, and the compliance of the pipes. Some tuning guidelines for the parameters K and B should be sought to reproduce the behaviors of actual systems by the presented simulation framework. In order to accelerate the computation, analytical methods for the root-finding routines that have appeared in the proposed algorithm in Sections 5 and 6 should also be addressed. Integration of the schemes of Sections 5 and 6, i.e., multiple actuators with regeneration pipelines driven by a single pump, is also an open problem.

References

- [1] V. Acary, O. Bonnefon, and B. Brogliato. Time-stepping numerical simulation of switched circuits within the nonsmooth dynamical systems approach. *IEEE Transactions on Computer-Aided Design of Integrated Circuits and Systems*, 29(7):1042–1055, 2010.
- [2] V. Acary and B. Brogliato. *Numerical Methods for Nonsmooth Dynamical Systems: Applications in Mechanics and Electronics*, volume 35 of *Lecture Notes in Applied and Computational Mechanics*. Springer, 2008.
- [3] K. Addi, S. Adly, B. Brogliato, and D. Goeleven. A method using the approach of Moreau and Panagiotopoulos for the mathematical formulation of non-regular circuits in electronics. *Nonlinear Analysis: Hybrid Systems*, 1(1):30–43, 2007.
- [4] W. Borutzky, B. Barnard, and J. Thoma. An orifice flow model for laminar and turbulent conditions. *Simulation Modelling Practice and Theory*, 10:141–152, 2002.
- [5] B. Brogliato, A. Daniilidis, C. Lemaréchal, and V. Acary. On the equivalence between complementarity systems, projected systems and differential inclusions. *Systems & Control Letters*, 55(1):45–51, 2006.
- [6] K. Choi, J. Seo, Y. Nam, and K. U. Kim. Energy-saving in excavators with application of independent metering valve. *Journal of Mechanical Science and Technology*, 29(1):387–395, 2015.
- [7] D. Christofori and A. Vacca. Modeling hydraulic actuator mechanical dynamics from pressure measured at control valve ports. *Proceedings of the Institution of Mechanical Engineers, Part I: Journal of Systems and Control Engineering*, 229(6):541–558, 2015.
- [8] M. C. Destro and V. J. De Negri. Method for combining valves with symmetric and asymmetric cylinders for hydraulic systems. *International Journal of Fluid Power*, 19(3):126–139, 2018.
- [9] B. Eriksson and J.-O. Palmberg. Individual metering fluid power systems: challenges and opportunities. *Proceedings of IMechE: Journal of Systems and Control Engineering*, 225(2):196–211, 2011.
- [10] A. Esposito. A simplified method for analyzing hydraulic circuits by analogy. *Machine Design*, 41(24):173–177, 1969.
- [11] D. Goeleven. Existence and uniqueness for a linear mixed variational inequality arising in electrical circuits with transistors. *Journal of Optimization Theory and Applications*, 138:397–406, 2008.
- [12] J. Greenslade, Thomas B. The hydraulic analogy for electric current. *Physics Teacher*, 41:464–466, 2003.
- [13] M. Kiani Oshtorjani, A. Mikkola, and P. Jalali. Numerical treatment of singularity in hydraulic circuits using singular perturbation theory. *IEEE/ASME Transactions on Mechatronics*, 24(1):144–153, 2018.
- [14] R. Kikuuwe. A sliding-mode-like position controller for admittance control with bounded actuator force. *IEEE/ASME Transactions on Mechatronics*, 19(5):1489–1500, 2014.

- [15] R. Kikuuwe. Anti-noise and anti-disturbance properties of differential-algebraic relaxation applied to a set-valued controller. In *Proceedings of the 15th International Workshop on Variable Structure Systems (VSS18)*, pages 480–485, 2018.
- [16] R. Kikuuwe. A brush-type tire model with nonsmooth representation. *Mathematical Problems in Engineering*, 2019:9747605, 2019.
- [17] R. Kikuuwe, N. Takesue, A. Sano, H. Mochiyama, and H. Fujimoto. Admittance and impedance representations of friction based on implicit Euler integration. *IEEE Transactions on Robotics*, 22(6):1176–1188, 2006.
- [18] R. Kikuuwe, S. Yasukouchi, H. Fujimoto, and M. Yamamoto. Proxy-based sliding mode control: A safer extension of PID position control. *IEEE Transactions on Robotics*, 26(4):670–683, 2010.
- [19] A. Lichtarowicz, R. K. Duggins, and E. Markland. Discharge coefficients for incompressible non-cavitating flow through long orifices. *Journal of Mechanical Engineering Science*, 7(2):210–219, 1965.
- [20] J. Rahikainen, F. González, M. Á. Naya, J. Sopenan, and A. Mikkola. On the cosimulation of multibody systems and hydraulic dynamics. *Multibody System Dynamics*, 50(2):143–167, 2020.
- [21] J. Rahikainen, M. Kiani, J. Sopenan, P. Jalali, and A. Mikkola. Computationally efficient approach for simulation of multibody and hydraulic dynamics. *Mechanism and Machine Theory*, 130:435–446, 2018.
- [22] J. Rahikainen, A. Mikkola, J. Sopenan, and J. Gerstmayr. Combined semi-recursive formulation and lumped fluid method for monolithic simulation of multibody and hydraulic dynamics. *Multibody System Dynamics*, 44:293–311, 2018.
- [23] M. Ruderman. Full- and reduced-order model of hydraulic cylinder for motion control. In *Proceedings of 43rd Annual Conference of IEEE Industrial Electronics Society (IECON 2017)*, pages 7275–7280, 2017.
- [24] S. Sakai and S. Stramigioli. Visualization of hydraulic cylinder dynamics by a structure preserving nondimensionalization. *IEEE/ASME Transactions on Mechatronics*, 23(5):2196–2206, 2018.
- [25] A. Shenouda. *Quasi-static hydraulic control systems and energy savings potential using independent metering four-valve assembly configuration*. PhD thesis, Georgia Institute of Technology, 2006.
- [26] A. Shenouda and W. Book. Optimal mode switching for a hydraulic actuator controlled with four-valve independent metering configuration. *International Journal of Fluid Power*, 9(1):35–43, 2008.
- [27] K. A. Tabor. A novel method of controlling a hydraulic actuator with four valve independent metering using load feedback. *SAE Technical Paper Series*, 2005-01-3639, 2005.
- [28] L. Wang, W. J. Book, and J. D. Huggins. Application of singular perturbation theory to hydraulic pump controlled systems. *IEEE/ASME Transactions on Mechatronics*, 17(2):251–259, 2012.

- [29] D. Wu, R. Burton, and G. Schoenau. An empirical discharge coefficient model for orifice flow. *International Journal of Fluid Power*, 3(3):13–10, 2002.
- [30] X. Xiong, R. Kikuuwe, and M. Yamamoto. A differential-algebraic method to approximate nonsmooth mechanical systems by ordinary differential equations. *Journal of Applied Mathematics*, 2013:320276, 2013.
- [31] X. Xiong, R. Kikuuwe, and M. Yamamoto. A multistate friction model described by continuous differential equations. *Tribology Letters*, 51(3):513–523, 2013.
- [32] J. Yao, Z. Jiao, D. Ma, and L. Yan. High-accuracy tracking control of hydraulic rotary actuators with modeling uncertainties. *IEEE/ASME Transactions on Mechatronics*, 19(2):633–641, 2014.
- [33] Y. Ye, C.-B. Yin, X.-D. Li, W.-J. Zhou, and F.-F. Yuan. Effects of groove shape of notch on the flow characteristics of spool valve. *Energy Conversion and Management*, 86:1091–1101, 2014.
- [34] A. Ylinen, H. Marjamäki, and J. Mäkinen. A hydraulic cylinder model for multibody simulations. *Computers and Structures*, 138(1):67–72, 2014.